

Original Article

Reduced expression of enolase-1 correlates with high intracellular glucose levels and increased senescence in cisplatin-resistant ovarian cancer cells

Yasmarié Santana-Rivera^{1,6}, Robert J Rabelo-Fernández^{2,6}, Blanca I Quiñones-Díaz^{3,6}, Nilmary Grafals-Ruíz^{4,6}, Ginette Santiago-Sánchez^{3,6}, Eunice L Lozada-Delgado^{2,6}, Ileabett M Echevarría-Vargas^{3,6}, Juan Apiz^{6,7}, Daniel Soto^{2,6}, Andrea Rosado^{1,6}, Loyda Meléndez^{5,6}, Fatima Valiyeva⁶, Pablo E Vivas-Mejía^{3,6}

Departments of ¹Interdisciplinary Sciences, ²Biology, University of Puerto Rico, Rio Piedras Campus, San Juan 00927, Puerto Rico; Departments of ³Biochemistry, ⁴Physiology, ⁵Microbiology and Medical Zoology, ⁶Comprehensive Cancer Center, University of Puerto Rico, Medical Sciences Campus, San Juan 00935, Puerto Rico; ⁷Department of Biology, University of Puerto Rico, Cayey Campus, Cayey 00736, Puerto Rico

Received January 9, 2020; Accepted March 10, 2020; Epub April 15, 2020; Published April 30, 2020

Abstract: Despite good responses to first-line treatment with platinum-based combination chemotherapy, most ovarian cancer patients will relapse and eventually develop a platinum-resistant disease with a poor overall prognosis. The molecular events leading to the cisplatin resistance of ovarian cancer cells are not fully understood. Here, we performed a proteomic analysis to identify protein candidates deregulated in a cisplatin-resistant ovarian cancer cell line (A2780CP20) in comparison to their sensitive counterpart (A2780). Forty-eight proteins were differentially abundant in A2780CP20, as compared with A2780, cells. Enolase-1 (ENO1) was significantly decreased in cisplatin-resistant ovarian cancer cells. Western blots and RT-PCR confirmed our findings. Ectopic ENO1 expression increased the sensitivity of ovarian cancer cells to cisplatin treatment. In contrast, small-interfering (siRNA)-based ENO1 silencing in A2780 cells reduced the sensitivity of these cells to cisplatin treatment. Whereas glucose consumption was lower, intracellular levels were higher in cisplatin-resistant ovarian cancer cells as compared with their cisplatin-sensitive counterparts. Senescence-associated β -galactosidase (β -Gal) levels were higher in cisplatin-resistant ovarian cancer cells as compared with cisplatin-sensitive ovarian cancer cells. β -Gal levels were decreased in ENO1 overexpressed clones. Protein levels of the cell cycle regulators and senescence markers p21 and p53 showed opposite expression patterns in cisplatin-resistant compared with cisplatin sensitive cells. Our studies suggest that decreased expression of ENO1 promotes glucose accumulation, induces senescence, and leads to cisplatin resistance of ovarian cancer cells.

Keywords: Enolase, ENO1, senescence, p21, p53, glucose, cisplatin resistance, ovarian cancer, beta-Gal

Introduction

Cytoreductive surgery and platinum/taxane combination chemotherapy are the most common treatments for patients with ovarian cancer [1]. Although the majority of ovarian cancer patients respond to front-line platinum combination chemotherapy, relapse occurs in over 60% of treated patients, resulting in chemoresistant fatal disease [1]. Several molecular mechanisms of cisplatin chemoresistance have been postulated, including decreased cisplatin accumulation inside cells, increased sulfur-cisplatin complexes and DNA repair mechanisms, the activation of anti-apoptotic signals and inactivation of pro-apoptotic pathways, and dys-

regulation of oncogenes, tumor suppressor genes, and non-coding RNAs [2, 3]. However, the key molecular pathways responsible for the cisplatin resistance of ovarian cancer cells have not been completely elucidated.

Evidence indicates that posttranscriptional and posttranslational regulation of gene expression governs the function of several proteins associated with cancer initiation, progression, and drug resistance. Recent advances in proteomics have made possible the simultaneous quantitative comparison of the proteome profile in drug-sensitive and drug-resistant cancer cells [4]. For example, Bruce and co-workers identified 374 proteins with significantly altered

expression levels in cisplatin-resistant cells as compared to cisplatin-sensitive HeLa cells [5]. Many of these proteins had not been previously associated with cisplatin resistance. Similarly, changes in protein abundance associated with the mitochondrial proteomes that promote evasion of apoptosis, tumor invasiveness, and metastasis of cisplatin-resistant epithelial ovarian cancer cells were reported [6]. Moreover, studies in ovarian cancer have also identified differential protein abundance in chemoresistant metastatic tissue and cell lines [4, 7]. This evidence indicates that proteomic approaches are useful in identifying key molecules in molecular pathways that contribute to cisplatin resistance in ovarian cancer.

Aiming to identify key proteins associated with cisplatin resistance in ovarian cancer, we performed a proteomic analysis in cisplatin-sensitive (A2780) and cisplatin-resistant (A2780-CP20) ovarian cancer cells. Results showed low levels of Enolase-1 (ENO1) in A2780CP20 compared to A2780 cells. Western blot and real-time PCR studies confirmed that ENO1 is significantly reduced in a panel of cisplatin-resistant ovarian cancer cells as compared with cisplatin-sensitive ovarian cancer cells. Because ENO1 is an enzyme involved in glucose metabolism, we measured the glucose consumption and the intracellular glucose levels and we observed lower glucose consumption in cisplatin-resistant compared with cisplatin-sensitive ovarian cancer cells. However, the intracellular glucose levels were higher in cisplatin-resistant cells than in cisplatin-sensitive cells. We further investigated how ENO1 silencing, or its overexpression, correlated with the intracellular glucose levels and with the sensitivity of these cells to cisplatin treatment. Finally, we measured beta-galactosidase (β -Gal) levels in cisplatin-resistant and cisplatin-sensitive ovarian cancer cells and we noted that β -Gal levels were lower in cisplatin-resistant ovarian cancer cells. β -Gal levels were also correlated with ENO1 expression levels. Western blot analysis showed that the levels of the cell cycle regulators and senescence markers p21 and p53 showed opposite expression patterns in cisplatin-resistant compared with cisplatin sensitive cells. Our studies suggest that the decreased expression of ENO1 promotes glucose accumulation, induces senescence, and increases cisplatin resistance in ovarian cancer cells.

Materials and methods

Cell lines and culture conditions

The human ovarian epithelial cancer cell lines A2780 and A2780CIS were purchased from the European Collection of Cell Cultures (ECACC). OV-90 and OVCAR3 cells were purchased from the American Type Culture Collection (ATCC). OV-90CIS and OVCAR3CIS were generated by exposing the parental cells to increasing concentrations of cisplatin. A2780CP20, HEYA8, and HEYA8-MDR were provided by Dr. Anil K. Sood (MD Anderson Cancer Center) and have been described elsewhere [8-11]. Each cell line was screened using Mycoplasma removal agent, as described by the manufacturer (AbD Serotec). For in vitro propagation, cells were maintained in RPMI-1640 medium (Thermo Scientific) alone (A2780, A2780CP20, A2780CIS, HEYA8, and HEYA8-MDR), or containing 0.01 mg/mL insulin (Sigma-Aldrich; OVCAR3 and OVCAR3CIS) or 0.5 mg/mL G418 (Sigma-Aldrich; Empty Vector and ENO1-overexpressing clones). OV-90 and OV-90CIS cells were maintained in M199 (Gibco, Life Technologies)/MCDB-105 (Sigma-Aldrich) medium. In all cases, the medium was supplemented with 10% fetal bovine serum (FBS; Thermo Scientific) and 0.1% antibiotic/antimycotic solution (Thermo Scientific). Cell lines and clones were grown at 37°C in 5% CO₂ with 95% air. In vitro experiments were performed at 70%-75% cell confluence. The concentration of cisplatin inhibiting 50% of cell growth (IC₅₀) was calculated by the Alamar Blue method 72 hours after the incubation of each cell line with cisplatin [11, 12].

Proteomics analysis

2-D Fluorescence Difference Gel Electrophoresis (2D-DIGE) analysis: The first and second dimension separation was performed as published by Ciborowski and coworkers with some modifications [13]. Briefly, first dimension separation was carried out with an IPGphor III apparatus (GE Healthcare). Protein cell extracts (500 μ g of A2780 and 500 μ g of A2780CP20) were loaded onto Immobiline DryStrips gels (24 cm long) with linear immobilized pH gradient 3-11 non-linear gradient (NL) and rehydrated overnight. Isoelectric focusing was performed at a constant temperature of 20°C with a total of 45 kVh. Strips were then incubated with an equilibration solution (50 mM Tris-HCL pH 8.8,

ENO1 expression in ovarian cancer cells

6 M urea, 30% glycerol, 2% SDS, 0.01% bromophenol blue) containing 100 mM DTT for 15 minutes. Gel strips were also incubated with 100 mM iodoacetamide in equilibration solution for 15 minutes to alkylate proteins. Then, the strips were loaded onto 12% polyacrylamide gels and fixed with 0.5% agarose. The second dimension separation was performed using an Ettan Dalttwelve Electrophoresis System (GE Healthcare) at 20°C. For visualization of protein spots, signals were collected at excitation wavelength for Cy2-, Cy3-, and Cy5-labeled samples at 488, 520, and 620 nm, respectively, using Ettan DIGE Imager (GE Healthcare). Gels were analyzed using DeCyder 2D 6.5 software (GE Healthcare). Spot normalization was done relative to the total volume of all spots in the whole gel. The protein spots with differences of 1.2-fold between A2780 and A2780CP20 cells (p -values < 0.05) were considered for MS identification. Protein spots selected for protein identification after DeCyder analysis were picked from preparative gels (loaded with 125 µg of protein extracts) using an automatic Ettan Spot Picker (GE Healthcare) with a 2.0 mm diameter picking head.

Preparation of peptide digests for identification by tandem mass spectrometry

Protein spots collected from preparative gels were washed at room temperature with 50% acetonitrile (ACN)/50 mM NH_4HCO_3 for 1 hour. Gel pieces were then dried in a speed vac and incubated with trypsin (Promega, Madison, WI) in 50 mM NH_4HCO_3 overnight at 37°C. Digested peptides were then extracted with 60% ACN and 0.1% trifluoroacetic acid (TFA), dried on a speed vac and resuspended in 0.5% TFA. All samples were purified using C18 ZipTips (Millipore) according to the manufacturer's recommendations and resuspended in 2% ACN with 0.1% formic acid prior to LC-MS/MS analysis.

Mass spectrometry and protein identification

Peptides were fractionated on a microcapillary RP-C18 column (NewObjectives) followed by fragmentation using ESI-LC-MS/MS system (ProteomeX System with LTQ, ThermoElectron, Inc.) in a nano-spray configuration. The spectra obtained from mass spectrometric analyses were searched using Sequest™ search engine (BioWorks 3.2 software from ThermoElectron Inc). In the TurboSEQUEST search parameters,

10,000 thresholds and 1.4 precursor mass tolerance for Dta generation were used. For Dta Search, we used a peptide tolerance of 1.5 and fragment ions tolerance of 0.02 with charge state set on "Auto". An indexed human.fasta.idx database with the following five keywords: Homo, sapiens, human, man, primate was created from nr.fasta retrieved from <http://ncbi.nih.gov>. Keratins and cytokeratins were excluded from our human.fasta.idx database. The protein identity was accepted only if the probability was a significant threshold level with $P \leq 0.05$, and at least two peptides matched.

Western blot analysis

Each cell line was detached with trypsin (0.25%) at 37°C, washed with Phosphate Buffer Saline (PBS), harvested, and stored at -80°C until processed. Cells were lysed with ice-cold lysis buffer (1% Triton X, 150 mM NaCl, 25 mM Tris HCl, 0.4 mM NaVO_4 , 0.4 mM NaF, and protease inhibitors) and incubated on ice for 30 min. Whole-cell lysates were centrifuged, supernatants were collected, and protein concentration was determined using Bio-Rad Protein Reagents. In all cases, protein lysates (30-50 µg) were separated by SDS-PAGE, blotted onto nitrocellulose membranes, and probed with the appropriate dilution of AL7A1 (ALDH7) (Abcam ab106815), PRDX6 (Abcam ab 59585), RL27 (RPL27) (Abcam ab94537), DOPD (DDT) (Abcam ab150338), ENOA (ENO1) (Sigma, AV3476), ILKAP (Abcam ab11857), CYTB (Sigma HPA017380), p21 (Cell Signaling 2974), and p53 (cell Signaling 2527) primary antibodies. Membranes were rinsed and incubated with horseradish peroxidase-conjugated secondary antibodies. Bound antibodies were detected using enhanced chemiluminescence (GE Healthcare) followed by autoradiography in a FluorChem™ 8900 (Alpha Innotech Corporation). Densitometry analysis of band intensities for each protein, including β -actin, was performed. Fold changes in protein levels were calculated, first relative to the β -actin (Sigma A5441), and then relative to the protein levels in A2780 cells that were taken as 1 in each replicate.

RNA isolation, cDNA synthesis, and SYBR-I-based real-time PCR analysis

Total RNA was isolated using the GenElute Mammalian Total RNA Miniprep kit from Sigma

ENO1 expression in ovarian cancer cells

Aldrich. RNA was converted into complementary DNA (cDNA) with the Enhanced Avian RT first strand synthesis kit from Sigma-Aldrich. In brief, total RNA (1 µg), 500 mM dNTP, 2.5 mM random nonamers, and nuclease-free water were mixed up to 10 mL total volume. The mixture was centrifuged and heated at 70°C for 10 minutes and combined with 1 mL of enhanced avian RT, 2 mL 10X buffer, 1 mL RNase inhibitor, and nuclease-free water up to 20 mL total volume. Samples were then preincubated at 25°C for 15 minutes, followed by incubation at 45°C for 50 minutes. SYBR-I-based Real-Time PCR (qPCR) was performed in a StepOne plus Real-Time PCR System (Thermo Scientific). In brief, 10 mL of Power SYBR Green PCR master mix reagent (Applied Biosystems), 0.5 mL of forward primer, 0.5 mL reverse primer (0.4 mM final concentration each), 2 mL of cDNA product, and nuclease-free water up to 20 mL final volume. Primers: ENO1 forward: GATCTCTCA-CCTCAAAGC, ENO1 reverse: TTCCATCCATCTC-GATCATC. Beta-actin (β-actin) was used as an endogenous control. Primers: β-actin forward: CCCTTTTGTCCCAAC, β-actin reverse: CTGG-TCTCAAGTCAGTGACAGG. Cycling conditions: one cycle of 10 minutes at 95°C, and 40 cycles of 15 seconds at 95°C, 30 seconds at 60°C and 30 seconds at 72°C. Melt curve analysis was performed at the end of the PCR reaction. Relative ENO1 expression was calculated with the $\Delta\Delta C_t$ -method [14, 15].

ENO1 stable transfection

Ectopic ENO1 expression was performed in A2780CP20 cells. ENO1 (ORF expression clone for ENO1, catalog # EX-C0061-M02, accession number: NM_001428) and Empty Vector (pReceiver-M02, catalog # EX-NEG-M02) were purchased from GeneCopoeia. In brief, A2780CP20 cells were seeded onto 6-well plates at a concentration of 3.5×10^4 cells/mL and incubated at 37°C, 5% CO₂. The next day, 2 µg of ENO1 or Empty Vector in combination with MegaTran 1.0 Transfection reagent (ratio 1:1.5 w/v) (OriGene, catalog # TT200002) was added to each well. Twenty-four hours later, the culture media was replaced by RPMI-1640-containing G418 (0.5 mg/mL) to select stable transfected clones. Individual clones were picked up and grown in independent flasks. ENO1 expression levels in each clone were measured by Western blot analysis.

Transient transfection of small-interfering RNA (siRNA)

Since the ENO1 gene is shared between two isoforms, ENO1 (NM_001428.5) and Myc binding protein 1 (MBP-1) (NM_001201483.3) [16], two different siRNA sequences were designed: siENO1(1) targets the ENO1 region 5'-GGTGC-TTCAACTGGTATCT-3'; while siENO1(2) targeted the ENO1 region 5'-AGATACCAGTTGAAGCACC-3', which is common for both ENO1 and MBP-1 isoforms. ENO1 siRNAs and negative control, siRNA (NC-siRNA), were purchased from Sigma. Prior to transfection, 1.5×10^5 cells/mL of A2780 were plated into 10 cm Petri dishes. Twenty-four hours later, siRNAs were mixed with HiPerfect transfection reagent (Qiagen) at a 1:2 ratio (siRNA: transfection reagent, vol/vol) and incubated at room temperature (RT) for 20 minutes. The mix was added drop by drop to the cells and allowed to be transfected at 37°C, 5% CO₂, and collected 24 hours later for Western blot analysis.

Cell viability and colony formation assays

For cell viability, A2780CP20-ENO1 or Empty Vector clones (2×10^4 cells/mL) were seeded into 96-well plates. The next day, cells were treated with different concentrations of cisplatin and incubated for 48 hours. For cell viability upon siRNA transfection, cells (3.5×10^4 cells/mL) were seeded into 96-well plates and the next day cells were transfected with 100 nM of siRNAs as described above. Twenty-four hours later, 2 mM cisplatin was added for an additional 48 hours. At the end of the treatment, the medium was removed and 95 µl of Alamar blue (Invitrogen) dye was added. OD values were obtained spectrophotometrically in a plate reader (BioRad) after a maximum of 4 hours of dye incubation. In all cases, percentages of cell viability were obtained after blank OD subtraction, taking the values of the untreated cells as a normalization control.

For colony formation assays, clones (3.5×10^4 cells/mL) were plated into 6-well plates, and the next day 2 mM cisplatin was added. Eight hours later, the media was removed and 1000 cells were seeded into 10 cm Petri dishes. Ten days later, colonies were stained with 0.5% crystal violet in methanol. Colonies of at least 50 cells were counted in five random fields (10X) using the Nikon Eclipse TS100 micro-

ENO1 expression in ovarian cancer cells

scope. The percentage of colonies was calculated relative to the number of colonies in the Empty Vector plate, which was considered as 100%.

Glucose consumption and intracellular glucose measurements

Glucose consumption was measured using a Gluc Cell glucose monitoring system (Thermo Fisher Scientific). Cells (3×10^4 cells/ml) were plated in 6-well plates, and the next day the culture media was replaced by fresh media. Two μ l of the media was taken directly from the cell culture supernatants, placed in the Test Strips, and inserted in the monitoring system. This procedure was done at 0, 12, 24, 48 and 72 h after adding fresh media. Immediately after each measurement, cells were collected and counted by the trypan blue method. Glucose levels were expressed in mg/dL and normalized to 100,000 cells. The intracellular glucose levels were measured with the Glucose Assay Kit from Abcam (catalog # AB65333) as per the manufacturer specifications. In brief, cells were washed with 1X PBS, detached with 0.25% of Trypsin, collected, and resuspended in cold 1X PBS at 1×10^6 cells/mL. Two million cells were lysed with Assay Buffer and deproteinized with a Deproteinizing Sample Preparation Kit (Abcam catalog # AB204708), according to the manufacturer specifications. Processed samples were analyzed by colorimetric measurements using a microplate reader (BioRad) at an OD of 570 nm. The amount of glucose in each sample was extrapolated from a glucose standard curve prepared for each experiment with known concentrations of glucose.

Senescence-associated β -galactosidase activity

Senescence was measured in a panel of ovarian cancer cells and A2780CP20 ENO1 clones with a beta-galactosidase (β -Gal) Detection Kit from Abcam (catalog # AB176721). This kit uses the fluorogenic fluorescein digalactoside (FDG) galactosidase substrate, which, upon cleavage by β -Gal, generates a fluorescent product that can be measured. In brief, cells were collected, lysed with protein lysis buffer (included in the kit), and diluted at 1 μ g/mL protein concentration. Protein aliquots of each sample were incubated with FDG for 4 hours. After this period of time, a stop buffer was added, and the fluorescence in each sample was quantified

with a Thermo Scientific Varioskan Flash spectral reader at 490 nm excitation and 525 nm emission. β -Gal levels in each sample were calculated using a β -galactosidase standard curve prepared for each experiment.

Statistical analysis

For *in vitro* and *in vivo* experiments, statistical analysis was performed using Student's t-test. *P*-values of <0.05 were considered statistically significant. GraphPad Prism software was used for graphing and statistical analysis.

Results

Proteomic analysis revealed several proteins differentially abundant in cisplatin-resistant and cisplatin-sensitive ovarian cancer cells

Following 2-DIGE protein separation and DeCyder analysis, protein spots with >1.2 -fold changes and *p*-values ≤ 0.05 were selected for protein identification by mass spectroscopy (MS). The MS data was analyzed and filtered using TurboSEQUEST with the following parameters: DelCn of 0.1, XCorr of 1.5 and 70% of protein coverage. By using these parameters, 147 proteins were identified ([Supplementary Table 1](#)). Forty-eight out of the 147 proteins were differentially abundant in cisplatin-resistant (A2780CP20), as compared with cisplatin-sensitive (A2780), cells ([Supplementary Table 2](#)). Based on the human.fasta.idx index, fold change (higher than 2-fold), and their biological roles, seven differentially abundant proteins, including ENOA (ENO1), ILKAP, RL27, PRDX6, CYTB, DOPD and AL7A1 (**Table 1**), were selected for further validation by Western blots.

Western blots and densitometric analysis of the band intensities showed non-significant differences in protein abundance between cisplatin-sensitive (A2780) and cisplatin-resistant (A2780CP20) ovarian cancer cells for RL27, CYTB, DOPD or AL7A1 (**Figure 1A, 1B**). The protein levels of PRDX6 showed the opposite tendency in the Western blots and the proteomic studies (**Figure 1A, 1B**). On the other hand, ILKAP and ENOA (ENO1) protein levels showed the same tendency in the Western blots and the proteomic studies (**Figure 1A, 1B**). ILKAP is a protein phosphatase that plays a role in the regulation of cell cycle progression via dephosphorylation of its substrates, primarily ILK [17-21]. The role of ILKAP and ILK in ovarian cancer

ENO1 expression in ovarian cancer cells

Table 1. Candidate proteins from the proteomics studies selected for further validation

Protein Symbol	Fold Change A2780CP20 vs A2780	Biological Role
ENOA	-2.69	Functions as a glycolytic enzyme. ENOA is also a multifunctional enzyme involved in growth control, cellular stress, parasitic infections, autoantigen activities, and cancer.
ILKAP	-2.52	Protein phosphatase that may play a role in regulation of cell cycle progression via dephosphorylation of its substrates.
RL27	+4.34	Part of the 60S subunit: DNA replication, transcription and repair, RNA splicing and modification.
PRDX6	+2.78	Mitochondrial protein Involved in redox regulation of cells; protects against oxidative injuries. It can reduce H ₂ O ₂ , short-chain organic, fatty acid, and phospholipid hydroperoxides.
CYTB	-2.67	Intracellular thiol proteinase inhibitor. Tightly binding reversible inhibitor of cathepsins L, H, and B.
DOPD	+5.07	Enzyme: Tautomerization of D-dopachrome with decarboxylation to give 5,6-dihydroxindole (DHI).
AL7A1	+2.74	Play a major role in the detoxification of aldehydes generated by alcohol metabolism and lipid peroxidation.

ENO1 expression in ovarian cancer cells

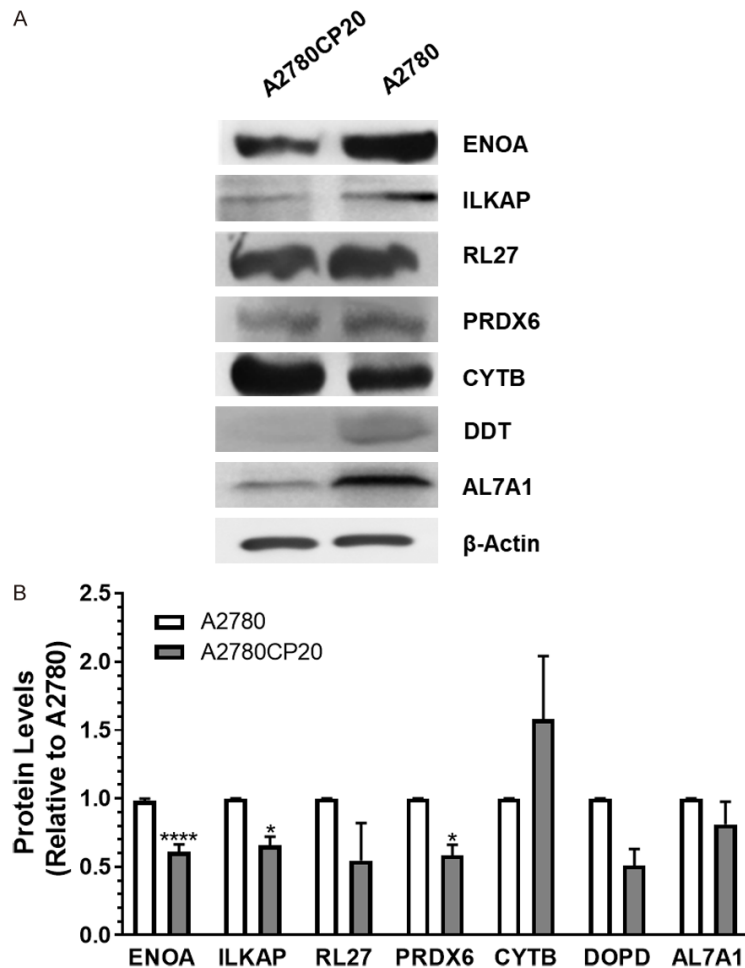


Figure 1. Western blot validation of the proteomic results. (A) Western blot analysis was performed using 30-50 μ g of protein extracts. Beta-Actin (β -actin) was used as a loading control. (B) Densitometry analysis of band intensities shown in (A). Fold changes in protein levels were calculated relative to A2780 cells. Averages \pm SEM are shown for three independent experiments. * $P < 0.05$, **** $P < 0.0001$.

has been studied elsewhere [20, 22-24]. However, the biological consequences of ENO1 downregulation in ovarian cancer cells and its association with cisplatin resistance have not been investigated.

ENO1 protein and mRNA levels are lower in cisplatin-resistant ovarian cancer cells as compared with cisplatin-sensitive ovarian cancer cells

To determine if the decreased expression of ENO1 also occurred in other cisplatin-resistant ovarian cancer cells, we performed Western blots and SYBR-I-based real-time PCR. [Supplementary Table 3](#) shows the cisplatin IC_{50} values for the panel of ovarian cancer cells used in this study. Our results confirmed that ENO1 pro-

tein levels were decreased in cisplatin-resistant ovarian cancer cell lines (A2780CP20, A2780CIS, OV-90CIS, and OVCAR3CIS) when compared with their cisplatin-sensitive counterparts (A2780, OV-90, and OVCAR3) (**Figure 2A**). OV-90 and OVCAR3 are high-grade serous ovarian cancer (HGSOC) cell lines [25, 26]. HGSOC is the most common and lethal of the ovarian cancer types [25, 26]. The densitometric analysis of the Western blot bands showed that the decreased ENO1 levels were significantly lower in cisplatin-resistant ovarian cancer cells than in cisplatin-sensitive ovarian cancer cells (**Figure 2B**). The MBP-1 (Myc binding protein 1) band intensity in all cell lines is negligible compared with ENO1 levels ([Supplementary Figure 1A](#)). MBP-1 is a nuclear isoform of ENO1 [27]. Quantitative PCR results showed that the mRNA levels of ENO1 also were significantly lower in cisplatin-resistant cells as compared with cisplatin-sensitive ovarian cancer cells (**Figure 2C**). These results suggest that ENO1 levels in cisplatin-resistant ovarian cancer cells are altered also at the transcriptional level.

ENO1 expression levels correlate with the sensitivity of ovarian cancer cells to cisplatin treatment

We evaluated the hypothesis that ENO1 expression levels are associated with the sensitivity of ovarian cancer cells to cisplatin treatment. ENO1 was stably transfected into A2780CP20 cells. **Figure 3A** is a Western blot to assess ENO1 protein levels in Empty Vector (EV) and ENO1-stable transfected clones. Ectopic ENO1 expression did not affect MBP-1 expression levels ([Supplementary Figure 1B](#)). **Figure 3B** is a cell viability experiment showing that the ENO1-clone-5 was more sensitive (IC_{50} 8.1 mM) to cisplatin treatment compared with the EV clone (IC_{50} 11.4 mM). In a colony formation assay, we observed a reduced number of colonies in the

ENO1 expression in ovarian cancer cells

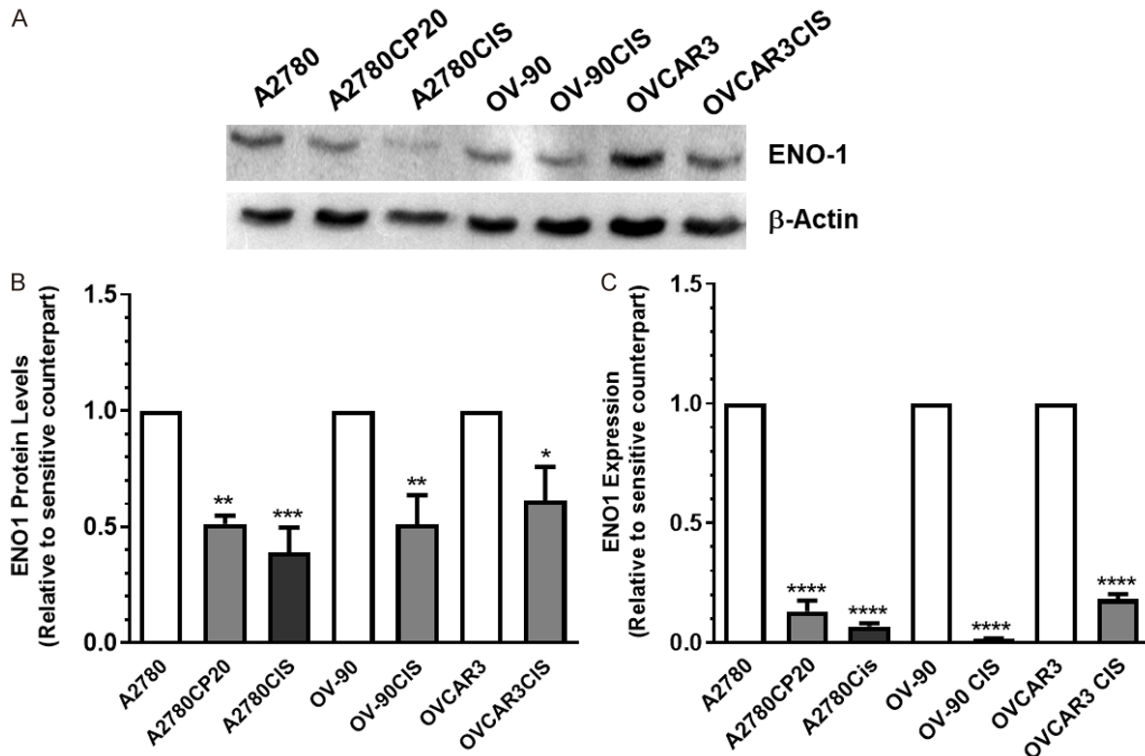


Figure 2. ENO1 protein and mRNA levels in a panel of ovarian cancer cells. (A) Western blot analysis was performed using protein extracts (30-50 μ g) of cisplatin-sensitive (A2780, OV-90, and OVCAR3) and cisplatin-resistant (A2780CP20, A2780CIS, OV-90CIS, and OVCAR3CIS) ovarian cancer cells. (B) Densitometry analysis of band intensities, shown in (A). Fold changes in protein levels were calculated relative to the cisplatin sensitive pair. Averages \pm SEM are shown for three independent experiments (C) ENO1 mRNA expression levels were assessed by qPCR. β -actin was used as a PCR internal control. Fold changes in mRNA levels were calculated relative to the cisplatin sensitive pair. Averages \pm SEM are shown for three independent experiments. * P <0.05, ** P <0.01, *** P <0.001, **** P <0.0001.

ENO1-clone-5 compared with the EV clone (**Figure 3C**). Importantly, cisplatin treatment reduced the number of colonies in almost 70% (**** P <0.0001) in the ENO1-clone-5 compared to the EV clone (**Figure 3D**). Images of the whole Petri dishes for the colony formation assay are shown in [Supplementary Figure 2](#).

Next, we transiently transfected A2780 cells with ENO1-targeted siRNAs. Since the ENO1 gene is shared between the two isoforms [16], ENO1 and MBP-1, two different siRNA sequences were designed: siENO1(1) targets the mRNA of ENO1 only; while siENO1(2) targets both the ENO1 and MBP-1 isoforms. **Figure 3E** is a Western blot showing that both siRNAs decreased ENO1 protein levels. **Figure 3F** shows the densitometric analysis of the band intensities of **Figure 3E**. We observed that both siRNAs were able to reduce the ENO1 protein levels [siENO1(1) *** P <0.001 and siENO1(2) **** P <0.0001] as compared with NC-siRNA-transfected cells. Furthermore, compared with the

NC-siRNA, the siENO1(1) reduced the sensitivity of A2780 cells to cisplatin treatment (2 mM final concentration) (**Figure 3G**). For example, at 100 nM of siRNA, the cell viability was 93% with the NC-siRNA and 97% with siENO1(1). When cells were exposed to cisplatin, the cell viability was 76% for NC-siRNA and 89% for siENO1(1) (**Figure 3G**). Transient transfection of the siRNA targeting both ENO1 and MBP-1 [siRNA(2)] did not induce significant changes in the sensitivity of A2780 cells to cisplatin treatment as compared with the NC-siRNA transfected cells ([Supplementary Figure 3](#)). Together, these results suggest that ENO1 levels correlate with the sensitivity of A2780 cells to cisplatin treatment.

Intracellular glucose levels are higher in cisplatin-resistant ovarian cancer cells than in cisplatin-sensitive ovarian cancer cells

ENO1 is a glycolytic enzyme responsible for catalyzing the conversion of 2-phosphoglycer-

ENO1 expression in ovarian cancer cells

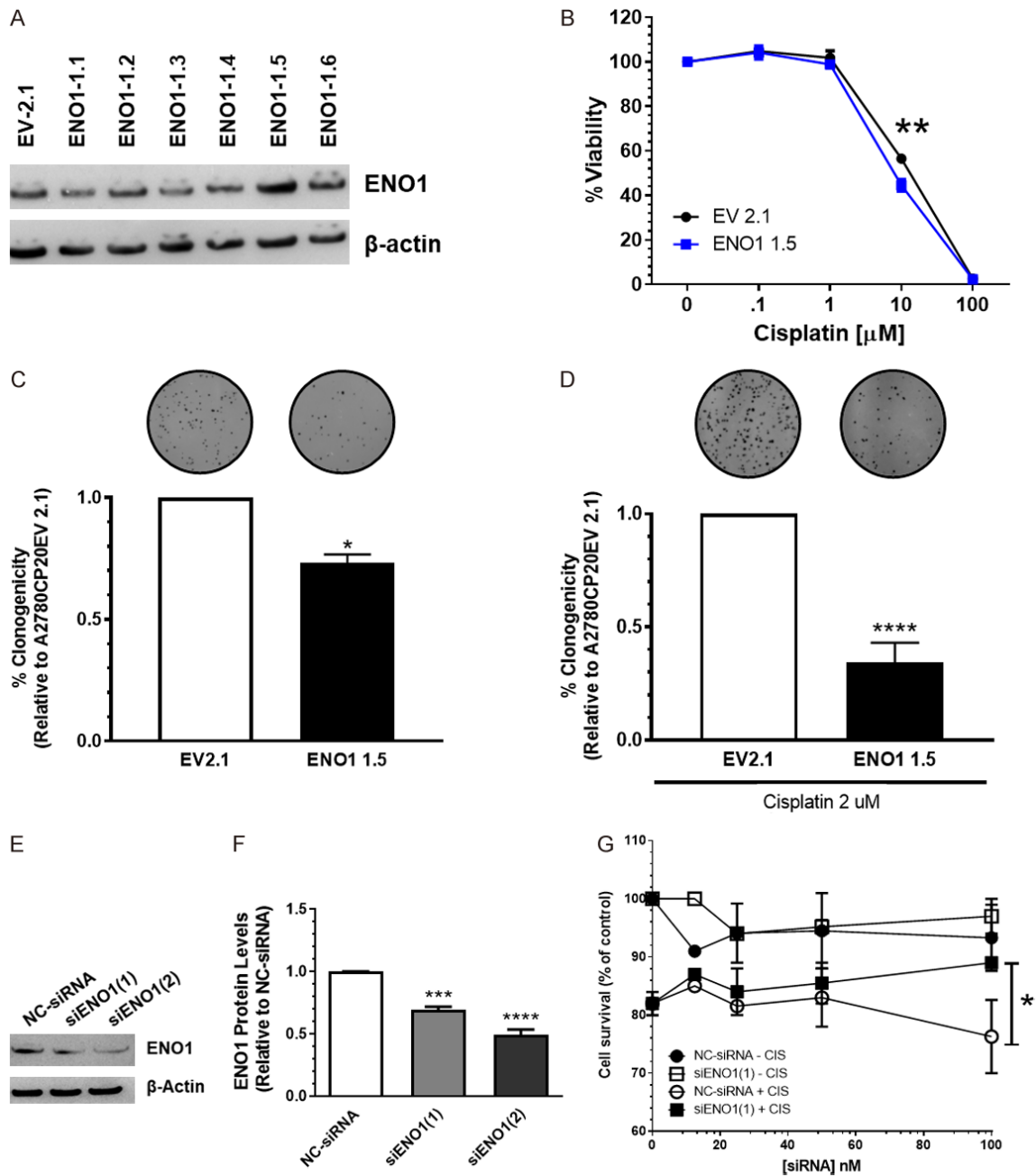


Figure 3. In vitro effect of ENO1 overexpression or silencing on cell growth and proliferation. (A) A2780CP20 cells were stably transfected with an empty vector (EV) or with an ENO1-containing vector. Western blot analysis was performed with 50 μ g of protein extracts. (B) EV and ENO1 clones (3×10^4 cell/ml) were exposed to different concentrations of cisplatin for 72 h. Cell viability values were calculated relative to untreated cells. (C, D) Percentages of clonogenicity were calculated relative to EV cells. (E) A2780 cells (3×10^4 cells/ml) were transiently transfected with a negative control siRNA (NC-siRNA) or the two ENO1-targeted siRNAs. Western blot was performed with 50 μ g of protein extracts. (F) Densitometry analysis of band intensities from (E). Protein levels were calculated relative to NT cells. (G) A2780 cells (3×10^4 cells/ml) cells were plated in 96-wells and the next day cells were transfected with different concentrations of siRNAs, as described in (E) Twenty-four hours after siRNA transfection, cisplatin (2 mM, final concentration) was added to the cells. Forty-eight hours later, cell viability was measured. Averages \pm SEM are shown for three independent experiments. * $P < 0.05$, ** $P < 0.01$, *** $P < 0.001$, **** $P < 0.0001$.

ate to phosphoenolpyruvate [27, 28]. Lack of the ENO1 enzyme promotes the intracellular

accumulation of glucose [27, 29]. Therefore, we assessed if ENO1 levels correlated with the

ENO1 expression in ovarian cancer cells

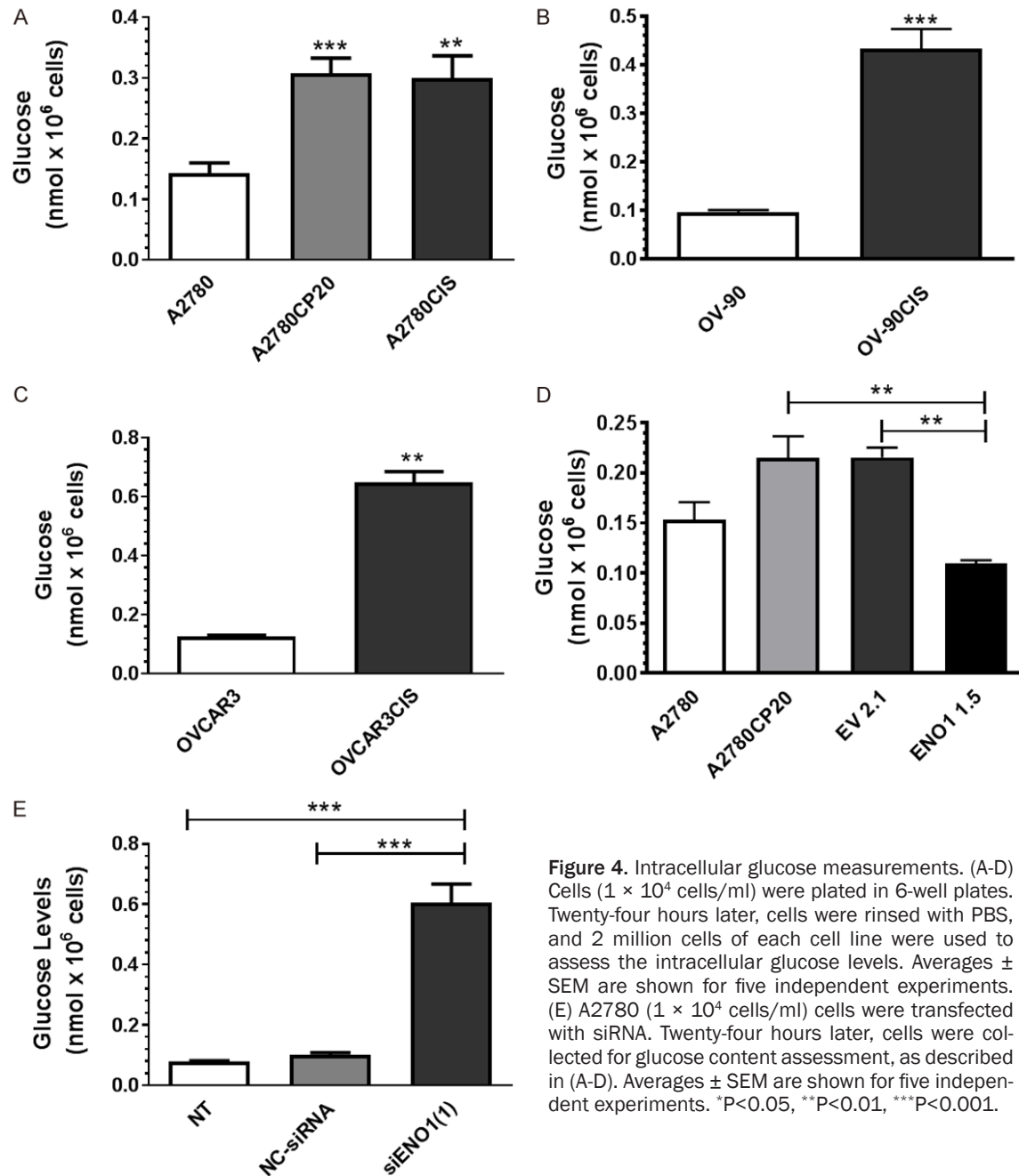


Figure 4. Intracellular glucose measurements. (A-D) Cells (1×10^4 cells/ml) were plated in 6-well plates. Twenty-four hours later, cells were rinsed with PBS, and 2 million cells of each cell line were used to assess the intracellular glucose levels. Averages \pm SEM are shown for five independent experiments. (E) A2780 (1×10^4 cells/ml) cells were transfected with siRNA. Twenty-four hours later, cells were collected for glucose content assessment, as described in (A-D). Averages \pm SEM are shown for five independent experiments. * $P < 0.05$, ** $P < 0.01$, *** $P < 0.001$.

intracellular glucose levels in cisplatin-sensitive cells and cisplatin-resistant ovarian cancer cells. **Figure 4A-C** show that the intracellular glucose levels were significantly higher in cisplatin-resistant than in cisplatin-sensitive cells. In addition, the intracellular glucose levels were significantly lower (** $P < 0.001$) in the ENO1-overexpressing clone as compared with the EV clone (**Figure 4D**). Moreover, the intracellular glucose levels were significantly higher (** $P < 0.001$) in siRNA-mediated ENO1 silenced cells

as compared with NC-siRNA transfected cells (**Figure 4E**).

Cisplatin resistant ovarian cancer cells consume less glucose than cisplatin sensitive ovarian cancer cells

As higher intracellular glucose levels in cisplatin-resistant cells may be caused by higher glucose consumption, we measured glucose consumption in the panel of ovarian cancer cells

ENO1 expression in ovarian cancer cells

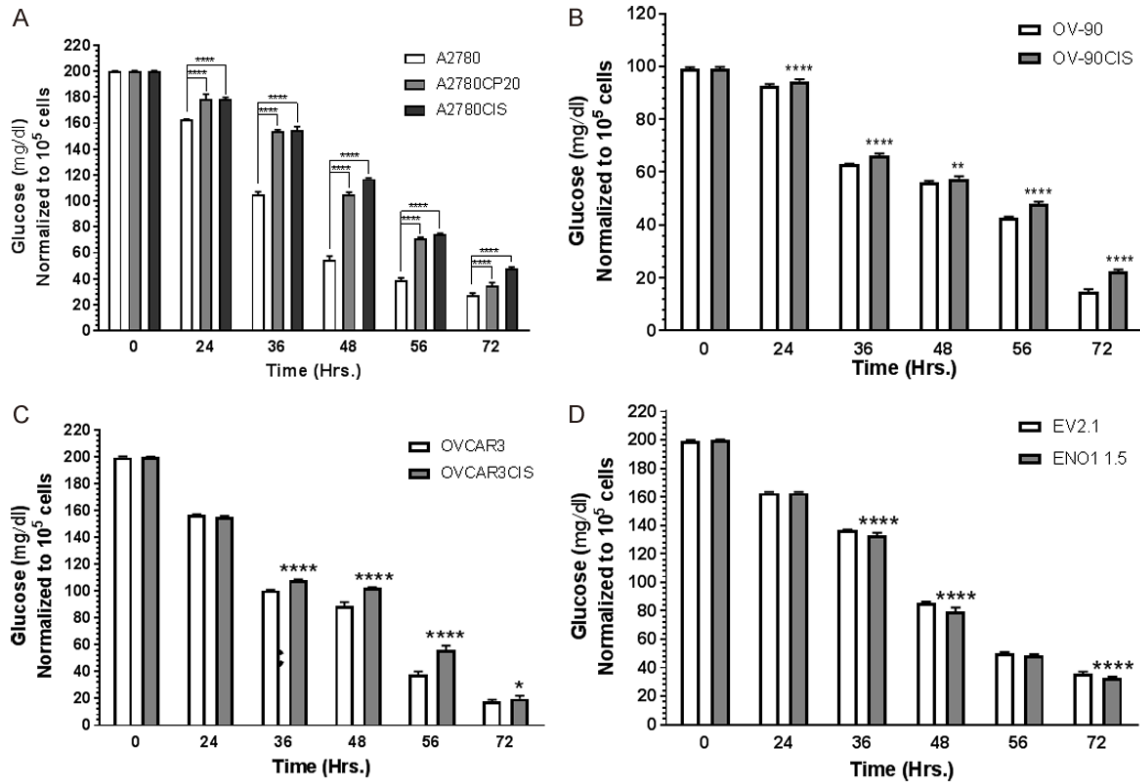


Figure 5. Glucose consumption measurements. A-D. Cells (1×10^4 cells/ml) were plated in 6-well plates. Glucose was measured in the cultured media. Averages \pm SEM are shown for three independent experiments. * $P < 0.05$, ** $P < 0.01$, *** $P < 0.001$, **** $P < 0.0001$.

and the ENO1 clones. **Figure 5** shows the glucose levels measured in the cultured media at different time points. In all cell lines tested, the glucose levels decreased in a time-dependent manner. However, cisplatin-resistant cells consumed a smaller glucose amount (higher glucose levels in the culture media) than their cisplatin sensitive counterparts at all time-points tested (**Figure 5A-C**). Although we observed statistically significant differences in the glucose levels between the EV and ENO1 clones (**Figure 5D**), these differences were minimal compared with the changes observed between the cisplatin-sensitive and the cisplatin-resistant ovarian cancer cells. Together, results showed in **Figures 4** and **5** indicate that, although cisplatin-resistant ovarian cancer cells consume less glucose, they accumulate higher amounts of it compared with cisplatin-sensitive cells.

Senescence-associated markers in ovarian cancer cells

Previous studies have shown that the acquisition of drug resistance is accompanied by a

senescence phenotype of cancer cells [30-32]. Evidence also indicates that decreased expression of ENO1 and high glucose intracellular levels promote cellular senescence [30]. Thus, we measured the senescence-associated beta-galactosidase (β -Gal) levels in cisplatin-resistant and cisplatin-sensitive ovarian cancer cells and the ENO1-overexpressing clone. **Figure 6A** shows that the β -Gal levels were significantly higher in the cisplatin-resistant cells compared with their cisplatin-sensitive counterparts. Importantly, the β -Gal levels decreased in the ENO1-overexpressing clone as compared with the EV clone (**Figure 6B**). Finally, we measured the levels of p21 and p53, cell cycle progression regulators and senescence-associated markers [31]. The Western blot image showed in **Figure 6C** indicates that the p21 protein levels were almost absent in cisplatin-resistant as compared with their cisplatin sensitive counterparts, where the p21 levels were prominent. Opposite tendency was observed for p53, as the levels of this protein was increased in cisplatin resistant as compared with cisplatin sensitive cells. Original Western blot images were

ENO1 expression in ovarian cancer cells

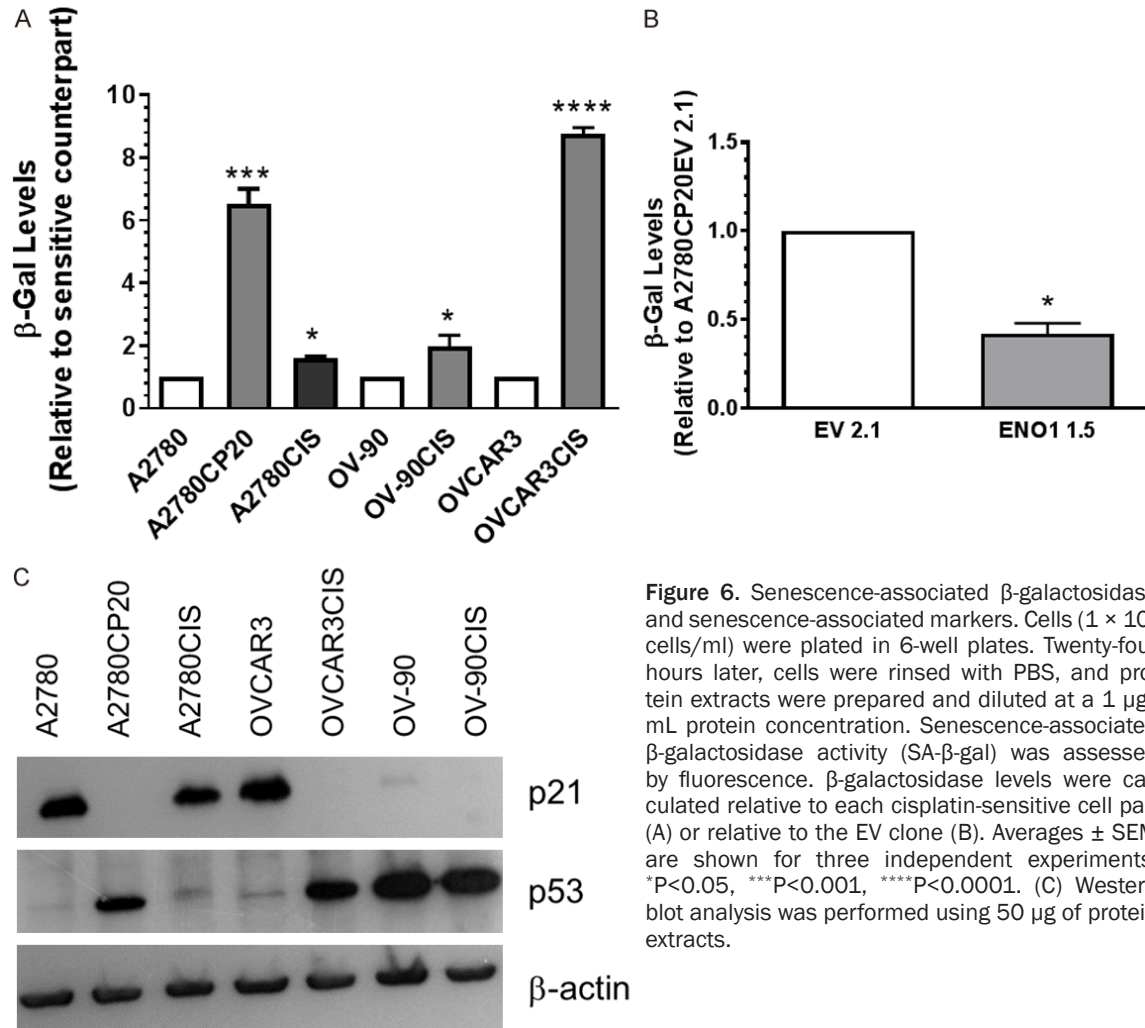


Figure 6. Senescence-associated β -galactosidase and senescence-associated markers. Cells (1×10^4 cells/ml) were plated in 6-well plates. Twenty-four hours later, cells were rinsed with PBS, and protein extracts were prepared and diluted at a $1 \mu\text{g}/\text{mL}$ protein concentration. Senescence-associated β -galactosidase activity (SA- β -gal) was assessed by fluorescence. β -galactosidase levels were calculated relative to each cisplatin-sensitive cell pair (A) or relative to the EV clone (B). Averages \pm SEM are shown for three independent experiments. * $P < 0.05$, *** $P < 0.001$, **** $P < 0.0001$. (C) Western blot analysis was performed using $50 \mu\text{g}$ of protein extracts.

included in the [Supplementary Figure 4](#). Of note, OV-90 cells exhibited low p21 and high p53 protein levels (**Figure 6C**). Together, these results suggest that decreased expression of ENO1 promotes senescence of cisplatin-resistant ovarian cancer cells by regulating p21 and p53 protein levels.

Discussion

By using a proteomic approach, we identified Enolase-1 (ENO1) as significantly decreased in cisplatin-resistant as compared with cisplatin-sensitive ovarian cancer cells. Our results were confirmed in HGSOc cells by using Western blot and qPCR. Although our proteomic analysis identified several proteins differentially abundant in cisplatin-sensitive and cisplatin-resistant ovarian cancer cells, Western blot analysis only confirmed the proteomic expression patterns for ILKAP and enolase- α (ENO α or ENO1).

The protein expression levels of the additional five proteins assessed using Western blots did not correlate with the proteomic results. One possible explanation for this observation is that the protein assessed by immunoblots was an isoform or a paralog of the protein identified by MS [33]. Another possibility is a misidentification of candidate proteins with the parameters used for protein searching and identification with the TurboSequest program [34]. For example, as we used only 70% of ion coverage, some spectra cannot be matched to the correct sequence and they could be erroneously assigned to a different peptide in the database [34]. Additionally, as many peptides in proteomic studies still have amino acid modifications, spectra derived from modified peptides are commonly assigned to the wrong amino acid sequences [35]. This problem commonly leads to false protein identifications and errors

ENO1 expression in ovarian cancer cells

in protein quantification [35]. Furthermore, poor protein digestion, highly hydrophilic or very small peptides that are not retained in a column or highly large/hydrophobic peptides that are stuck in gel or are too large for mass spectrometer analysis, also could contribute to inaccuracies in our proteomic data [35]. In any case, future studies could explore the role of other differentially abundant proteins ([Supplementary Table 2](#)) in cisplatin-resistant and cisplatin-sensitive ovarian cancer cells.

Enolases are metalloenzymes responsible for the conversion of 2-phosphoglycerate (2-PG) to phosphoenolpyruvate (PEP) during glycolysis [27, 28]. ENO1 (ENO- α) is one of three enolase isoforms, the other two being ENO2 (ENO- γ) and ENO3 (ENO- β) [28]. Besides glycolysis, ENO1 is a multifunctional enzyme involved in growth control, cellular stress, parasitic infections, autoantigen activities, cancer metastasis and drug resistance [28]. ENO1 is also present on the surface of several cell types, such as leukocytes and neurons where it serves as a receptor and activator of plasminogen [28]. In our study, decreased ENO1 levels were associated with intracellular glucose accumulation and senescence of cisplatin-resistant ovarian cancer cells. These results are in agreement with information stating that, besides metabolism control, ENO1 is a key enzyme involved in cell growth, survival and drug resistance, and that all of these events are intimately associated with each other [28].

The reduced protein levels of ENO1 in cisplatin-resistant cells were confirmed using HGSOC cell (OVCAR3/OVCAR3CIS and OV-90/OV-90CIS) pairs. As HGSOC is the most common and malignant of the gynecological cancers [1], our findings suggest that reduced ENO1 protein levels could be used as a predictor of drug response in women with HGSOC. This hypothesis should be confirmed at the protein level by immunohistochemical (IHC) experiments with HGSOC patient samples. When we interrogated the KM Plotter database (www.kmplot.com) which includes close to 1600 ovarian cancer samples we observed that ovarian cancer patients with low ENO1 mRNA levels recur faster (PFS) than patients with high ENO1 mRNA levels (data not shown). However, this correlation was not statistically significant. Our findings that mRNA levels are reduced in cisplatin-resistant cells suggest the absence/repression of transcription factors responsible for ENO1

expression. Oncogenes such as RAS, MYC, and HIF-1 α have been reported to increase ENO1 expression [16, 30, 36]. However, we and others have shown that these transcription factors are overexpressed/mutated in cisplatin-resistant ovarian cancer cells [16, 36, 37]. It could be speculated that a repressor protein is responsible for the reduced expression of ENO1 in cisplatin-resistant ovarian cancer cells. The identification of this protein is crucial to fully understand how ENO1 is regulated in ovarian cancer cells. Interestingly, in a proteomic study, Kotz et al. found that ENO1 is associated with the fluorescent carboxy-fluorescein-diacetate-labelled cisplatin analog (CFDA-cisplatin) in A2780 and A2780CIS cells [38]. This interaction might decrease the net intracellular cisplatin levels and contribute to the drug resistance of ovarian cancer cells. This hypothesis should be further investigated.

Alternative splicing of the ENO1 mRNA transcript generates a cytoplasmic protein (ENO1) or a nuclear protein referred to as Myc-binding protein-1 (MBP-1) [16, 39]. Subramanian and Miller reported that MBP-1 binds to the P2 promoter DNA region of c-MYC and down-regulates c-MYC expression [39]. As c-MYC levels are highly abundant in cisplatin-resistant ovarian cancer cells [37], the negligible expression levels of MBP-1 in ovarian cancer cells could partially contribute to the high c-MYC levels observed in those cells [37]. In fact, when we used the siRNA to reduce the expression of ENO1 only, cells become less sensitive to cisplatin treatment. However, when we used the siRNA targeting, both ENO1 and MBP-1, changes in cisplatin sensitivity were not observed. These results could be due to the elimination of the c-MYC repression by MBP-1 [16]. Because designing siRNAs targeting only MBP-1 is particularly difficult (as the mRNA sequence of MBP-1 spans the same mRNA region of ENO1), the role of MBP-1 in ovarian cancer should be investigated with other, different approaches. Nevertheless, when we ectopically expressed ENO1 in cisplatin-resistant ovarian cancer cells, these cells became more sensitive to cisplatin treatment. Together, these results indicate that the decreased expression of ENO1 contributes to the cisplatin resistance of ovarian cancer cells.

The role of ENO1 in cancer is controversial. Liu and co-workers found that ENO1 overexpression positively correlated with clinical stage,

ENO1 expression in ovarian cancer cells

lymph node metastasis, and poor prognosis of patients with pancreatic cancer [40]. Qi and co-workers reported that the mRNA and protein levels of ENO1 were upregulated in glioma tissues compared to normal brains [41]. ShRNA-mediated ENO1 knocking-down decreased cell proliferation, inhibited cell migration and invasion; and reduced *in vivo* tumorigenesis of glioma cells [41]. Elevated expression of ENO1 has also been observed in cell lines and tissue samples of breast, lung, prostate, and pancreatic cancers, as well as in neuroendocrine tumors, neuroblastoma, cholangiocarcinoma, thyroid carcinoma, hepatocellular carcinoma, and Burkitt lymphoma [27]. In contrast, a proteomic study performed by Auer et al. in endometrioid endometrial cancer samples found that ENO1 was decreased as compared with normal controls [42]. By using Western blotting and IHC analysis, Mao and co-workers reported that ENO1 is frequently down-regulated in non-small cell lung cancer (NSCLC) tissue patients, and its down-regulation correlated with aggressive tumor behavior [43]. An explanation for the discrepancy regarding ENO1 expression is not currently available. Changes in ENO1 levels by cellular stress [27], the occurrence of the MBP-1 isoform and ENO1 pseudogenes, the abundance of microRNAs (miRNAs) post-transcriptionally controlling ENO1 protein expression [29], and the presence of heterogeneous cell populations in a tumor might contribute to the opposing ENO1 levels reported in the literature. Particularly, Jin and co-workers found that reduced expression of miR-22 increases ENO1 expression levels, stimulates glycolysis, and promotes cisplatin resistance in gastric cancer cells [29]. If cisplatin-resistant ovarian cancer cells express higher levels of miR-22 than their cisplatin sensitive counterparts, this could explain the opposite findings of Jin and co-workers and our findings. In fact, while, in some cancers, miR-22 acts as a tumor suppressor gene, in other tumors it exhibits oncogenic properties [44]. Thus, studies to clarify if ENO1 is post-transcriptionally regulated by non-coding RNAs in ovarian cancer should be performed. Nevertheless, our findings that ENO1 was decreased in cisplatin-resistant ovarian cancer cells compared with cisplatin-sensitive ovarian cancer cells are in agreement with reports that lower levels of ENO1 lead to intracellular glucose accumulation, senescence, and the selection of certain cell populations which are more resistant to chemotherapy [30, 45, 46].

Another important finding of our study was that cisplatin-resistant cells consume less glucose than their cisplatin-sensitive counterparts. Possible explanations for this finding include the decreased levels of glucose transporters that reduce the influx of cisplatin to the inside of cells. Two types of glucose transport have been described: sodium-glucose linked transporters (SGLTs) and facilitated diffusion glucose transporters (GLUT) [47]. Six members of the SGLT and twelve members of the GLUT transports have been reported [47]. Ishiko and co-workers assessed the expression of GLUT1, GLUT3, and GLUT4 in human ovarian tumor samples using immunohistochemical analysis, and observed that the expressions of GLUT1 and GLUT4 correlated with the tumor stage, and the expressions of GLUT1, GLUT3 and GLUT4 correlated positively with VEGF expression [48]. More recently, Fang and co-workers used a GLUT1-specific inhibitor and observed *in vitro* inhibition of cell proliferation and *in vivo* tumor reduction with ovarian cancer cell line- and patient-derived xenograft mouse models [49]. Further studies should measure the expression levels of all of these receptors in cisplatin-sensitive and cisplatin-resistant ovarian cancer cells. The differences in glucose consumption rates were higher in A2780CP20/A2780CIS/A2780 than in OV-90CIS/OV-90 or OVCAR3CIS/OVCAR3 pairs of cells. Although A2780 is classified as an endometrial ovarian cancer (EOC) cell line [25] and would not present a good model of HGSOC [25, 50], these cells are still used to study molecular mechanisms of cisplatin resistance [37]. Yet, differences in gene expression between EOC and HGSOC could account for the observed differences in glucose consumption rates. Additionally, A2780CP20 and A2780CIS are ~50 and ~8 times more resistant, respectively, to cisplatin than A2780 cells. However, OV-90CIS and OVCAR3CIS are only 3-times and 4.5-times more resistant than OV-90 and OVCAR3, respectively, to cisplatin treatment ([Supplementary Table 3](#)) which could also account for the differences in glucose consumption rates we observed. Our findings that cisplatin-resistant cells also contain higher intracellular glucose levels than their sensitive counterparts support our hypothesis that the reduced expression of ENO1 avoids the glucose consumption in cisplatin-resistant cells. Importantly, Avril and co-workers found that, opposite to cisplatin sensitive cells, cisplatin-

ENO1 expression in ovarian cancer cells

resistant ovarian cancer cells rely on glutamine more than glucose as their main energy source [51]. Future experiments could address how glutamine-dependent metabolism leads to the senescence of cisplatin-resistant ovarian cancer cells.

Novelli and co-workers studied the role of ENO1 in the Warburg effect [30]. The Warburg effect, also known as aerobic glycolysis, is a characteristic of most solid tumors, increasing the glycolysis rate both in hypoxic conditions and in the presence of normal oxygen level, independent of mitochondrial status [52, 53]. Novelli and co-workers used shRNA-mediated ENO1 depleted cells and observed increases in reactive oxygen species (ROS) which were generated through the sorbitol and NADPH oxidase pathways [30]. Interestingly, ENO1 silenced cells are forced to use glucose through the pentose phosphate and the polyol pathways, with a consequent decrease in lactate levels [30]. ENO1 silencing leads to cell cycle arrest in the G2/M phase and induced senescence [30]. In agreement with these results, we observed higher levels of intracellular glucose and senescence-associated β -Gal in cisplatin-resistant compared with cisplatin-sensitive cells that correlated with ENO1 expression levels. In fact, the effects of overexpressing ENO1 were more dramatic on clonogenic than in cell viability assays. The clonogenic assays measure long-term effects on cell proliferation, which include changes in gene expression, a step required for the acquisition of a senescence phenotype, as we observed in the cisplatin-resistant ovarian cancer cells. Together, our results suggest that the decreased expression of ENO1 in cisplatin-resistant ovarian cancer cells is part of their metabolic rewiring, a hallmark of cancer cells that includes re-programming for the optimal use of molecular precursors of proteins, lipids, and nucleotides required to maintain the enhanced growth, proliferation and metastatic potential of those cells [54].

Pillai and co-workers working with breast cancer cells and breast tumors obtained after neoadjuvant chemotherapy observed that oxidative stress caused by chemotherapeutic agents generated senescent-like colonies with an aggressive tumor stem cell-like phenotype [46]. These cells contained low levels of reactive oxygen species (ROS), high levels of antioxidant enzymes, and displayed higher CD133 and

Oct-4 expression. Our findings are in agreement with the hypothesis of Pillai and co-workers [46] and Chen and co-workers that, although therapy-induced senescence has short-term benefits, the response also causes the reprogramming of gene expression which leads to the selection of highly drug-resistant phenotype clones [45]. Although increased p21 and decreased p53 protein levels are associated with a senescence phenotype [31] we observed opposite tendency, as the p21 protein levels were reduced while the p53 levels were increased in cisplatin-resistant as compared with cisplatin sensitive cells. Downregulation of p21 and upregulation of p53 could promote a senescent drug-resistant phenotype in cancer cells. These hypotheses should be further investigated.

In conclusion, using quantitative proteomics and Western blot analysis, we demonstrated that ENO1 was reduced in cisplatin-resistant ovarian cancer cells as compared with cisplatin-sensitive ovarian cancer cells. ENO1 overexpression sensitized cells to cisplatin treatment, decreased the glucose intracellular levels, and reduced the senescence of cisplatin-resistant ovarian cancer cells. Molecules in pathways leading to the restoration of ENO1 levels could be considered as targets to design specific therapies to overcome the cisplatin resistance of ovarian cancer cells.

Acknowledgements

This research was funded by RCMI grant U54 MD007600 (National Institute on Minority Health and Health Disparities) from the National Institutes of Health, institutional seed funds from the University of Puerto Rico Comprehensive Cancer Center (PEVM), and the NIGMS-RISE Grant Number R25-GM061838 (NGR, BIQD, GSS, ELLD, IMEV). We would like to thank Mary Helen Mays, Ph.D. for critical reading and scientific editing of the manuscript and Juliana Perez-Laspiur, Ph.D. for running proteomic samples.

Disclosure of conflict of interest

None.

Address correspondence to: Dr. Pablo E Vivas-Mejía, Department of Biochemistry, University of Puerto Rico Comprehensive Cancer Center, Lab-8,

ENO1 expression in ovarian cancer cells

San Juan 00935, Puerto Rico. E-mail: pablo.vivas@upr.edu

References

- [1] Matulonis UA, Sood AK, Fallowfield L, Howitt BE, Sehouli J and Karlan BY. Ovarian cancer. *Nat Rev Dis Primers* 2016; 2: 16061.
- [2] Shen DW, Pouliot LM, Hall MD and Gottesman MM. Cisplatin resistance: a cellular self-defense mechanism resulting from multiple epigenetic and genetic changes. *Pharmacol Rev* 2012; 64: 706-721.
- [3] Damia G and Brogginini M. Platinum resistance in ovarian cancer: role of DNA repair. *Cancers (Basel)* 2019; 11.
- [4] Cruz IN, Coley HM, Kramer HB, Madhuri TK, Safuwani NA, Angelino AR and Yang M. Proteomics analysis of ovarian cancer cell lines and tissues reveals drug resistance-associated proteins. *Cancer Genomics Proteomics* 2017; 14: 35-51.
- [5] Chavez JD, Hoopmann MR, Weisbrod CR, Takara K and Bruce JE. Quantitative proteomic and interaction network analysis of cisplatin resistance in HeLa cells. *PLoS One* 2011; 6: e19892.
- [6] Chappell NP, Teng PN, Hood BL, Wang G, Darcy KM, Hamilton CA, Maxwell GL and Conrads TP. Mitochondrial proteomic analysis of cisplatin resistance in ovarian cancer. *J Proteome Res* 2012; 11: 4605-4614.
- [7] Coscia F, Watters KM, Curtis M, Eckert MA, Chiang CY, Tyanova S, Montag A, Lastra RR, Lengyel E and Mann M. Integrative proteomic profiling of ovarian cancer cell lines reveals precursor cell associated proteins and functional status. *Nat Commun* 2016; 7: 12645.
- [8] Behrens BC, Hamilton TC, Masuda H, Grotzinger KR, Whang-Peng J, Louie KG, Knutsen T, McKoy WM, Young RC and Ozols RF. Characterization of a cis-diamminedichloroplatinum(II)-resistant human ovarian cancer cell line and its use in evaluation of platinum analogues. *Cancer Res* 1987; 47: 414-418.
- [9] Landen CN Jr, Goodman B, Katre AA, Steg AD, Nick AM, Stone RL, Miller LD, Mejia PV, Jennings NB, Gershenson DM, Bast RC Jr, Coleman RL, Lopez-Berestein G and Sood AK. Targeting aldehyde dehydrogenase cancer stem cells in ovarian cancer. *Mol Cancer Ther* 2010; 9: 3186-3199.
- [10] Vivas-Mejia P, Benito JM, Fernandez A, Han HD, Mangala L, Rodriguez-Aguayo C, Chavez-Reyes A, Lin YG, Carey MS, Nick AM, Stone RL, Kim HS, Claret FX, Bornmann W, Hennessy BT, Sanguino A, Peng Z, Sood AK and Lopez-Berestein G. c-Jun-NH2-kinase-1 inhibition leads to antitumor activity in ovarian cancer. *Clin Cancer Res* 2010; 16: 184-194.
- [11] Vivas-Mejia PE, Rodriguez-Aguayo C, Han HD, Shahzad MM, Valiyeva F, Shibayama M, Chavez-Reyes A, Sood AK and Lopez-Berestein G. Silencing survivin splice variant 2B leads to antitumor activity in taxane-resistant ovarian cancer. *Clin Cancer Res* 2011; 17: 3716-3726.
- [12] Larson EM, Doughman DJ, Gregerson DS and Obritsch WF. A new, simple, nonradioactive, nontoxic in vitro assay to monitor corneal endothelial cell viability. *Invest Ophthalmol Vis Sci* 1997; 38: 1929-1933.
- [13] Rozek W, Ricardo-Dukelow M, Holloway S, Gendelman HE, Wojna V, Melendez LM and Ciborowski P. Cerebrospinal fluid proteomic profiling of HIV-1-infected patients with cognitive impairment. *J Proteome Res* 2007; 6: 4189-4199.
- [14] Vargas IM and Vivas-Mejia PE. Assessment of mRNA splice variants by qRT-PCR. *Methods Mol Biol* 2013; 1049: 171-186.
- [15] Schmittgen TD and Livak KJ. Analyzing real-time PCR data by the comparative C(T) method. *Nat Protoc* 2008; 3: 1101-1108.
- [16] Feo S, Arcuri D, Piddini E, Passantino R and Giallongo A. ENO1 gene product binds to the c-myc promoter and acts as a transcriptional repressor: relationship with Myc promoter-binding protein 1 (MBP-1). *FEBS Lett* 2000; 473: 47-52.
- [17] Lorenzato A, Torchiario E, Olivero M and Di Renzo MF. The integrin-linked kinase-associated phosphatase (ILKAP) is a regulatory hub of ovarian cancer cell susceptibility to platinum drugs. *Eur J Cancer* 2016; 60: 59-68.
- [18] Hausmann C, Temme A, Cordes N and Eke I. ILKAP, ILK and PINCH1 control cell survival of p53-wildtype glioblastoma cells after irradiation. *Oncotarget* 2015; 6: 34592-34605.
- [19] Nakrieko KA, Vespa A, Mason D, Irvine TS, D'Souza SJ and Dagnino L. Modulation of integrin-linked kinase nucleocytoplasmic shuttling by ILKAP and CRM1. *Cell Cycle* 2008; 7: 2157-2166.
- [20] Kumar AS, Naruszewicz I, Wang P, Leung-Hagesteijn C and Hannigan GE. ILKAP regulates ILK signaling and inhibits anchorage-independent growth. *Oncogene* 2004; 23: 3454-3461.
- [21] Leung-Hagesteijn C, Mahendra A, Naruszewicz I and Hannigan GE. Modulation of integrin signal transduction by ILKAP, a protein phosphatase 2C associating with the integrin-linked kinase, ILK1. *EMBO J* 2001; 20: 2160-2170.
- [22] Ghatak S, Morgner J and Wickstrom SA. ILK: a pseudokinase with a unique function in the integrin-actin linkage. *Biochem Soc Trans* 2013; 41: 995-1001.
- [23] Ahmed N, Riley C, Oliva K, Stutt E, Rice GE and Quinn MA. Integrin-linked kinase expression increases with ovarian tumour grade and is sustained by peritoneal tumour fluid. *J Pathol* 2003; 201: 229-237.

ENO1 expression in ovarian cancer cells

- [24] Hannigan G, Troussard AA and Dedhar S. Integrin-linked kinase: a cancer therapeutic target unique among its ILK. *Nat Rev Cancer* 2005; 5: 51-63.
- [25] Domcke S, Sinha R, Levine DA, Sander C and Schultz N. Evaluating cell lines as tumour models by comparison of genomic profiles. *Nat Commun* 2013; 4: 2126.
- [26] Hernandez L, Kim MK, Lyle LT, Bunch KP, House CD, Ning F, Noonan AM and Annunziata CM. Characterization of ovarian cancer cell lines as in vivo models for preclinical studies. *Gynecol Oncol* 2016; 142: 332-340.
- [27] Ji H, Wang J, Guo J, Li Y, Lian S, Guo W, Yang H, Kong F, Zhen L, Guo L and Liu Y. Progress in the biological function of alpha-enolase. *Anim Nutr* 2016; 2: 12-17.
- [28] Diaz-Ramos A, Roig-Borrellas A, Garcia-Melero A and Lopez-Aleman R. alpha-Enolase, a multifunctional protein: its role on pathophysiological situations. *J Biomed Biotechnol* 2012; 2012: 156795.
- [29] Qian X, Xu W, Xu J, Shi Q, Li J, Weng Y, Jiang Z, Feng L, Wang X, Zhou J and Jin H. Enolase 1 stimulates glycolysis to promote chemoresistance in gastric cancer. *Oncotarget* 2017; 8: 47691-47708.
- [30] Capello M, Ferri-Borgogno S, Riganti C, Chataragada MS, Principe M, Roux C, Zhou W, Petricoin EF, Cappello P and Novelli F. Targeting the Warburg effect in cancer cells through ENO1 knockdown rescues oxidative phosphorylation and induces growth arrest. *Oncotarget* 2016; 7: 5598-5612.
- [31] Gordon RR and Nelson PS. Cellular senescence and cancer chemotherapy resistance. *Drug Resist Updat* 2012; 15: 123-131.
- [32] Rebbaa A. Targeting senescence pathways to reverse drug resistance in cancer. *Cancer Lett* 2005; 219: 1-13.
- [33] Chandramouli K and Qian PY. Proteomics: challenges, techniques and possibilities to overcome biological sample complexity. *Hum Genomics Proteomics* 2009; 2009.
- [34] Kim MS, Zhong J and Pandey A. Common errors in mass spectrometry-based analysis of post-translational modifications. *Proteomics* 2016; 16: 700-714.
- [35] Bogdanow B, Zauber H and Selbach M. Systematic errors in peptide and protein identification and quantification by modified peptides. *Mol Cell Proteomics* 2016; 15: 2791-2801.
- [36] Ying H, Kimmelman AC, Lyssiotis CA, Hua S, Chu GC, Fletcher-Sanankone E, Locasale JW, Son J, Zhang H, Coloff JL, Yan H, Wang W, Chen S, Viale A, Zheng H, Paik JH, Lim C, Guimaraes AR, Martin ES, Chang J, Hezel AF, Perry SR, Hu J, Gan B, Xiao Y, Asara JM, Weissleder R, Wang YA, Chin L, Cantley LC and DePinho RA. Oncogenic Kras maintains pancreatic tumors through regulation of anabolic glucose metabolism. *Cell* 2012; 149: 656-670.
- [37] Reyes-Gonzalez JM, Armaiz-Pena GN, Mangala LS, Valiyeva F, Ivan C, Pradeep S, Echevarria-Vargas IM, Rivera-Reyes A, Sood AK and Vivas-Mejia PE. Targeting c-MYC in platinum-resistant ovarian cancer. *Mol Cancer Ther* 2015; 14: 2260-2269.
- [38] Kotz S, Kullmann M, Kalayda GV, Dyballa-Rukes N, Jaehde U and Metzger S. Optimized two-dimensional gel electrophoresis in an alkaline pH range improves the identification of intracellular CFDA-cisplatin-protein adducts in ovarian cancer cells. *Electrophoresis* 2018; 39: 1488-1496.
- [39] Subramanian A and Miller DM. Structural analysis of alpha-enolase. Mapping the functional domains involved in down-regulation of the c-myc protooncogene. *J Biol Chem* 2000; 275: 5958-5965.
- [40] Yin H, Wang L and Liu HL. ENO1 overexpression in pancreatic cancer patients and its clinical and diagnostic significance. *Gastroenterol Res Pract* 2018; 2018: 3842198.
- [41] Song Y, Luo Q, Long H, Hu Z, Que T, Zhang X, Li Z, Wang G, Yi L, Liu Z, Fang W and Qi S. Alpha-enolase as a potential cancer prognostic marker promotes cell growth, migration, and invasion in glioma. *Mol Cancer* 2014; 13: 65.
- [42] Lomnyska MI, Becker S, Gemoll T, Lundgren C, Habermann J, Olsson A, Bodin I, Engström U, Hellman U, Hellman K, Hellström AC, Andersson S, Mints M and Auer G. Impact of genomic stability on protein expression in endometrioid endometrial cancer. *Br J Cancer* 2012; 106: 1297-1305.
- [43] Chang YS, Wu W, Walsh G, Hong WK and Mao L. Enolase-alpha is frequently down-regulated in non-small cell lung cancer and predicts aggressive biological behavior. *Clin Cancer Res* 2003; 9: 3641-3644.
- [44] Wang J, Li Y, Ding M, Zhang H, Xu X and Tang J. Molecular mechanisms and clinical applications of miR-22 in regulating malignant progression in human cancer (Review). *Int J Oncol* 2017; 50: 345-355.
- [45] Yang L, Fang J and Chen J. Tumor cell senescence response produces aggressive variants. *Cell Death Discov* 2017; 3: 17049.
- [46] Achuthan S, Santhoshkumar TR, Prabhakar J, Nair SA and Pillai MR. Drug-induced senescence generates chemoresistant stemlike cells with low reactive oxygen species. *J Biol Chem* 2011; 286: 37813-37829.
- [47] Navale AM and Paranjape AN. Glucose transporters: physiological and pathological roles. *Biophys Rev* 2016; 8: 5-9.
- [48] Tsukioka M, Matsumoto Y, Noriyuki M, Yoshida C, Nobeyama H, Yoshida H, Yasui T, Sumi T, Honda K and Ishiko O. Expression of glucose

ENO1 expression in ovarian cancer cells

- transporters in epithelial ovarian carcinoma: correlation with clinical characteristics and tumor angiogenesis. *Oncol Rep* 2007; 18: 361-367.
- [49] Ma Y, Wang W, Idowu MO, Oh U, Wang XY, Temkin SM and Fang X. Ovarian cancer relies on glucose transporter 1 to fuel glycolysis and growth: anti-tumor activity of BAY-876. *Cancers (Basel)* 2018; 11.
- [50] Viscarra T, Buchegger K, Jofre I, Riquelme I, Zanella L, Abanto M, Parker AC, Piccolo SR, Roa JC, Ili C and Brebi P. Functional and transcriptomic characterization of carboplatin-resistant A2780 ovarian cancer cell line. *Biol Res* 2019; 52: 13.
- [51] Hudson CD, Savadelis A, Nagaraj AB, Joseph P, Avril S, DiFeo A and Avril N. Altered glutamine metabolism in platinum resistant ovarian cancer. *Oncotarget* 2016; 7: 41637-41649.
- [52] Warburg O, Wind F and Negelein E. The metabolism of tumors in the body. *J Gen Physiol* 1927; 8: 519-530.
- [53] Liberti MV and Locasale JW. The Warburg effect: how does it benefit cancer cells? *Trends Biochem Sci* 2016; 41: 211-218.
- [54] Fouad YA and Aanei C. Revisiting the hallmarks of cancer. *Am J Cancer Res* 2017; 7: 1016-1036.

ENO1 expression in ovarian cancer cells

Supplementary Table 1. List of the 147 proteins detected by proteomics in A2780 and A2780CP20 cells

UniProtKB	Protein Symbol	Protein Name	Gene Name	Location	Function
P62258	1433E	14-3-3 protein epsilon	YWHAE	Nucleus, Cytoplasm	Host-virus Interaction
P01889	1B07	HLA class I histocompatibility antigen, B-7 alpha chain	HLA-B	Membrane, MCH I	Host-virus Interaction, Immunity
P28223	5HT2A	5-hydroxytryptamine receptor 2A	HTR2A	Plasma Membrane	G-protein Coupled Receptor, Host Cell Receptor for Virus Entry, Receptor, Transducer
P52209	6PGD	6-phosphogluconate dehydrogenase, decarboxylating	PGD	Cytoplasm	Oxidoreductase
P29274	AA2AR	Adenosine receptor A2a	ADORA2A	Cell Membrane, Membrane	G-Protein Coupled Receptor, Receptor, Transducer
Q9UBJ2	ABCD2	ATP-binding cassette sub-family D member 2	ABCD2	Membrane, Peroxisome	ATPase activity, Transport
P49753	ACOT2	Acyl-coenzyme A thioesterase 2, mitochondrial	ACOT2	Mitochondrion	Hydrolase, Serine Esterase
P60709	ACTB	Actin, cytoplasmic 1	ACTB	Cytoplasm, Cytoskeleton, Nucleus	Motility
P68133	ACTS	Actin, alpha skeletal muscle	ACTA1	Cytoplasm, Cytoskeleton	Muscle Protein
Q9P0K1	ADA22	Disintegrin and metalloproteinase domain-containing protein 22	ADAM22	Cell Membrane, Cell Projection, Membrane	Receptor
Q16186	ADRM1	Proteasomal ubiquitin receptor ADRM1	ADRM1	Cytoplasm, Nucleus, Proteasome	Protein regulation
Q02952	AKA12	A-kinase anchor protein 12	AKAP12	Cytoplasm, Cytoskeleton, Membrane	Anchoring Protein
P31749	AKT1	RAC-alpha serine/threonine-protein kinase	AKT1	Cell Membrane, Cytoplasm, Membrane, Nucleus	Developmental Protein, Kinase, Serine/Threonine-protein Kinase, Transferase
P49419	AL7A1	Alpha-aminoadipic semialdehyde dehydrogenase	ALDH7A1	Cytoplasm, Mitochondrion, Nucleus	Oxidoreductase
P04075	ALDOA	Fructose-bisphosphate aldolase A	ALDOA	Cytoplasm	Lyase
Q9GZV1	ANKR2	Ankyrin repeat domain-containing protein 2	ANKRD2	Cytoplasm, Nucleus	Transcription Regulator
P08243	ASNS	Asparagine synthetase [glutamine-hydrolyzing]	ASNS	Cytosol	Ligase
P25705	ATPA	ATP synthase subunit alpha, mitochondrial	ATP5F1A	Cell Membrane, CF(1), Membrane, Mitochondrion, Mitochondrion Inner Membrane	ATP Synthesis, Hydrogen Ion Transport, Ion transport, Transporter
UniProtKB	Protein Symbol	Protein Name	Gene Name	Location	Function
O00154	BACH	Cytosolic acyl coenzyme A thioester hydrolase	ACOT7	Mitochondrion, Cytoplasm	Hydrolase, Serine Esterase
O75531	BAF	Barrier-to-autointegration factor	BANF1	Chromosome, Cytoplasm, Nucleus	DNA-binding
Q13112	CAF1B	Chromatin assembly factor 1 subunit B	CHAF1B	Nucleus, Cytoplasm	Cell Cycle, DNA Damage, DNA Repair, DNA Replication, Transcription, Transcription Regulation
Q01518	CAP1	Adenylyl cyclase-associated protein 1	CAP1	Cell Membrane, Membrane	Actin-Binding
P49662	CASP4	Caspase-4	CASP4	Cytoplasm, Endoplasmic Reticulum, Inflammasome, Membrane, Mitochondrion, Extracellular Region	Hydrolase, Protease, Thiol Protease
P09668	CATH	Pro-cathepsin H	CTSH	Lysosome	Hydrolase, Protease, Thiol Protease
P52907	CAZA1	F-actin-capping protein subunit alpha-1	CAPZA1	Cytoplasm, Cytoskeleton	Actin Capping, Actin-binding
P04234	CD3D	T-cell surface glycoprotein CD3 delta chain	CD3D	Cell Membrane, Membrane	Receptor
P53567	CEBPG	CCAAT/enhancer-binding protein gamma	CEBPG	Nucleus	Activator, DNA-binding
P68400	CSK21	Casein kinase II subunit alpha	CSNK2A1	Nucleus	Kinase, Serine/Threonine-protein Kinase, Transferase
P04080	CYTB	Cystatin-B	CSTB	Nucleus, Cytoplasm	Protease Inhibitor, Thiol Protease Inhibitor
Q13561	DCTN2	Dynactin subunit 2	DCTN2	Cytoplasm, Cytoskeleton, Dynein, Membrane, Microtubule	Protein binding

ENO1 expression in ovarian cancer cells

P35659	DEK	Protein DEK	DEK	Nucleus	Chromatin Regulator, DNA-binding
P00367	DHE3	Glutamate dehydrogenase 1, mitochondrial	GLUD1	Mitochondrion	Oxidoreductase
P78352	DLG4	Disks large homolog 4	DLG4	Cell junction, Cell membrane, Cell projection, Cytoplasm, Membrane, Postsynaptic Cell Membrane, Synapse	Receptor Signaling
P30046	DOPD	D-dopachrome decarboxylase	DDT	Cytoplasm	Lyase
UniProtKB	Protein Symbol	Protein Name	Gene Name	Location	Function
P50570	DYN2	Dynamamin-2	DNM2	Cell Junction, Cell Membrane, Cell Projection, Coated Pit, Cytoplasm, Cytoplasmic vesicle, Cytoskeleton, Membrane, Microtubule, Postsynaptic Cell Membrane, Synapse	Hydrolase, Motor Protein
P49411	EFTU	Elongation factor Tu, mitochondrial	TUFM	Mitochondrion	Elongation factor
P00533	EGFR	Epidermal growth factor receptor	EGFR	Golgi Apparatus, Plasma Membrane, Nucleus, Endosome, Endoplasmic Reticulum, Extracellular Region	Developmental Protein, Host Cell Receptor for Virus Entry, Kinase, Receptor, Transferase, Tyrosine-protein Kinase
Q8N8S7	ENAH	Protein enabled homolog	ENAH	Cell Junction, Cell Projection, Cytoplasm, Cytoskeleton, Synapse	Actin-binding
P06733	ENOA	Alpha-enolase	ENO1	Cell membrane, Cytoplasm, Membrane, Nucleus	DNA-binding, Lyase, Repressor
Q9H6S3	ESSL2	Epidermal growth factor receptor kinase substrate 8-like protein 2	EPSL2	Cell Projection, Cytoplasm	Actin-binding
Q14296	FASTK	Fas-activated serine/threonine kinase	FASTK	Mitochondrion	Kinase, RNA-binding, Serine/Threonine-protein Kinase, Transferase
P07332	FES	Tyrosine-protein kinase Fes/Fps	FES	Cell Junction, Cell Membrane, Cytoplasm, Cytoplasmic Vesicle, Cytoskeleton, Golgi Apparatus, Membrane	Kinase, Transferase, Tyrosine-protein Kinase
Q02790	FKBP4	Peptidyl-prolyl cis-trans isomerase FKBP4	FKBP4	Cell Projection, Cytoplasm, Cytoskeleton, Microtubule, Mitochondrion, Nucleus	Chaperone, Isomerase, Rotamase
Q04446	GLGB	1,4-alpha-glucan-branching enzyme	GBE1	Cytosol, Extracellular Region	Glycosyltransferase, Transferase
P63096	GNAI1	Guanine nucleotide-binding protein G(i) subunit alpha-1	GNAI1	Cell Membrane, Cytoplasm, Cytoskeleton, Membrane, Nucleus	Transducer
P36969	GPX4	Phospholipid hydroperoxide glutathione peroxidase	GPX4	Cytoplasm, Mitochondrion	Developmental Protein, Oxidoreductase, Peroxidase
Q16836	HCDH	Hydroxyacyl-Coenzyme A dehydrogenase, Mitochondrial	HADH	Mitochondrion	Oxidoreductase
UniProtKB	Protein Symbol	Protein Name	Gene Name	Location	Function
P51858	HDGF	Hepatoma-derived growth factor	HDGF	Cytoplasm, Nucleus	DNA-binding, Repressor, Growth factor, Heparin-binding
P02790	HEMO	Hemopexin	HPX	Extracellular Region	Host-virus Interaction, Transport
P04233	HG2A	HLA class II histocompatibility antigen gamma chain	CD74	Endosome, Lysosome, Golgi Apparatus, Endoplasmic Reticulum, Plasma Membrane	Chaperone
Q16665	HIF1A	Hypoxia-inducible factor 1-alpha	HIF1A	Cytoplasm, Nucleus	Activator, DNA-binding
O75330	HMMR	Hyaluronan mediated motility receptor	HMMR	Cytoplasm	Hyaluronic Acid
P07910	HNRPC	Heterogeneous nuclear ribonucleoprotein C1/C2	HNRNPC	Nucleus, Spliceosome	Ribonucleoprotein, RNA-binding
Q00613	HSF1	Heat shock factor protein 1	HSF1	Nucleus, Cytoskeleton	Activator, DNA binding
Q03933	HSF2	Heat shock factor protein 2	HSF2	Nucleus, Cytoplasm	Activator, DNA-binding
P34932	HSP74	Heat shock 70 kDa protein 4	HSPA4	Cytoplasm	Stress Response

ENO1 expression in ovarian cancer cells

Q92839	HYAS1	Hyaluronan synthase 1	HAS1	Membrane	Glycosyltransferase, Transferase
Q92819	HYAS2	Hyaluronan synthase 2	HAS2	Membrane	Glycosyltransferase, Transferase
P05198	IF2A	Eukaryotic translation initiation factor 2 subunit 1	EIF2S1	Cytoplasm	Initiation Factor, RNA-binding
P35225	IL13	Interleukin 13	IL13	Extracellular Region	Cytokine
P05112	IL4	Interleukin-4	IL4	Extracellular Region	Cytokine, Growth Factor
Q13418	ILK	Integrin-linked protein kinase	ILK	Cell Junction, Cell Membrane, Cell Projection, Cytoplasm, Membrane	Kinase, Serine/Threonine-protein Kinase, Transferase
Q9H0C8	ILKAP	Integrin-linked kinase-associated serine/threonine phosphatase 2C	ILKAP	Cytoplasm	Hydrolase, Protein Phosphatase
P12268	IMDH2	Inosine-5'-monophosphate dehydrogenase 2	IMPDH2	Nucleus, Cytoplasm	DNA-binding, Oxidoreductase, RNA-binding
P41236	IPP2	Protein phosphatase inhibitor 2	PPP1R2	Nucleus, Cytosol	Protein Phosphatase Inhibitor
Q9Y624	JAM1	Junctional adhesion molecule A	F11R	Plasma Membrane	Host Cell Receptor for Virus Entry, Receptor
P56470	LEG4	Galectin-4	LGALS4	Extracellular Region, Cytosol, Plasma Membrane	Lectin
P02545	LMNA	Prelamin-A/C	LMNA	Intermediate Filament, Nucleus	Nucleus dynamics
Q02779	M3K10	Mitogen-activated protein kinase kinase kinase 10	MAP3K10	Cytoplasm	Kinase, Serine/Threonine-protein Kinase, Transferase
UniProtKB	Protein Symbol	Protein Name	Gene Name	Location	Function
Q99558	M3K14	Mitogen-activated protein kinase kinase kinase 14	MAP3K14	Cytoplasm	Kinase, Serine/Threonine-protein kinase, Transferase
Q9Y2U5	M3K2	Mitogen-activated protein kinase kinase kinase 2	MAP3K2	Nucleus, Cytoplasm	Kinase, Serine/Threonine-protein Kinase, Transferase
P40925	MDHC	Malate dehydrogenase, cytoplasmic	MDH1	Cytoplasm	Oxidoreductase
P28482	MK01	Mitogen-activated protein kinase 1	MAPK1	Nucleus, Cytoskeleton, Cytoplasm, Membrane	DNA-binding, Kinase, Repressor, Serine/Threonine-protein Kinase, Transferase
P27361	MK03	Mitogen-activated protein kinase 3	MAPK3	Cytoplasm, Membrane, Nucleus	Kinase, Serine/Threonine-protein kinase, Transferase
P01106	MYC	Myc proto-oncogene protein	MYC	Nucleus	Activator, DNA-binding
P04198	MYCN	N-myc proto-oncogene protein	MYCN	Nucleus	Activator, DNA-binding
Q15746	MYLK	Myosin light chain kinase, smooth muscle	MYLK	Cytoskeleton, Cell Projection, Cytoplasm	Actin-binding, Calmodulin-binding, Kinase, Serine/Threonine-protein Kinase, Transferase
P19878	NCF2	Neutrophil cytosol factor 2	NCF2	Cytoplasm	Electron transfer
Q15080	NCF4	Neutrophil cytosol factor 4	NCF4	Endosome, Cytoplasm, Membrane	Lipid-binding
O43639	NCK2	Cytoplasmic protein NCK2	NCK2	Endoplasmic Reticulum, Cytoplasm	Translation Regulation
P22392	NDKB	Nucleoside diphosphate kinase B	NME2	Cell Projection, Cytoplasm, Nucleus	Activator, DNA-binding, Kinase, Transferase
Q15843	NEDD8	NEDD8	NEDD8	Nucleus	Ubl Conjugation Pathway
Q16236	NF2L2	Nuclear factor erythroid 2-related factor 2	NFE2L2	Nucleus, Cytoplasm	Activator, DNA-binding
P19838	NFKB1	Nuclear factor NF-kappa-B p105 subunit	NFKB1	Nucleus, Cytoplasm	Activator, DNA-binding
Q9Y5S8	NOX1	NADPH oxidase 1	NOX1	Cell Junction, Cell Membrane, Cell Projection, Membrane	Ion channel, Oxidoreductase, Voltage-gated Channel
O14786	NRP1	Neuropilin-1	NRP1	Cell Membrane, Extracellular Region, Membrane	Developmental Protein, Heparin-binding, Receptor
P49757	NUMB	Protein numb homolog	NUMB	Membrane	Developmental Protein
Q9POS3/ Q53FV1	ORML1/ ORML2	ORM1-like protein 1/ORM1-like protein 2	ORMDL1/ ORMDL2	Endoplasmic Reticulum, Membrane	Metabolism

ENO1 expression in ovarian cancer cells

P04637	P53	Cellular tumor antigen p53	TP53	Nucleus, Cytoplasm, Endoplasmic Reticulum, Mitochondrion	Activator, DNA-binding, Repressor
UniProtKB	Protein Symbol	Protein Name	Gene Name	Location	Function
Q8WX93	PALLD	Palladin	PALLD	Cytoskeleton, Cell Projection, Cell Junction, Cytoplasm	Actin-binding
Q96R10	PAR4	Proteinase-activated receptor 4	F2RL3	Cell Membrane	G-protein Coupled Receptor, Receptor, Transducer
P23760	PAX3	Paired box protein Pax-3	PAX3	Nucleus	Developmental Protein, DNA-binding
Q01064	PDE1B	Calcium/calmodulin-dependent 3',5'-cyclic nucleotide phosphodiesterase 1B	PDE1B	Cytoplasm	Calmodulin-binding, Hydrolase
Q8IZL8	PELP1	Proline-, glutamic acid- and leucine-rich protein 1	PELP1	Nucleus, Cytoplasm	Activator, Repressor
P40855	PEX19	Peroxisomal biogenesis factor 19	PEX19	Peroxisome, Cytoplasm, Membrane	Peroxisome Biogenesis
P28328	PEX2	Peroxisome biogenesis factor 2	PEX2	Peroxisome, Membrane	Peroxisome Biogenesis
Q96HS1	PGAM5	Serine/threonine-protein phosphatase PGAM5, mitochondrial	PGAM5	Mitochondrion, Membrane, Mitochondrion Outer Membrane	Hydrolase
Q9Y3A3	PHOCN	MOB-like protein phocein	MOB4	Cytoplasm, Golgi Apparatus, Membrane	Transport
P42336	PK3CA	Phosphatidylinositol 4,5-bisphosphate 3-kinase catalytic subunit alpha isoform	PIK3CA	Cytosol, Plasma Membrane	Kinase, Serine/Threonine-protein Kinase, Transferase
O14939	PLD2	Phospholipase D2	PLD2	Membrane	Hydrolase
Q15435	PP1R7	Protein phosphatase 1 regulatory subunit 7	PPP1R7	Nucleus	Regulator enzyme
Q07869	PPARA	Peroxisome proliferator-activated receptor alpha	PPARA	Nucleus	Activator, DNA-binding, Receptor
P53041	PPP5	Serine/threonine-protein phosphatase 5	PPP5C	Cell Membrane, Nucleus, Cytoplasm, Membrane, Amyloid	Hydrolase, Protein Phosphatase
P30041	PRDX6	Peroxioredoxin-6	PRDX6	Lysosome, Cytoplasm	Antioxidant, Hydrolase, Multifunctional Enzyme, Oxidoreductase, Peroxidase
P07737	PROF1	Profilin-1	PFN1	Cytoskeleton, Cytoplasm	Actin-binding
P43686	PR56B	26S proteasome regulatory subunit 6B	PSMC4	Nucleus, Cytoplasm, Proteasome	ATP-binding, Nucleotide-binding
Q9UNM6	PSD13	26S proteasome non-ATPase regulatory subunit 13	PSMD13	Cytosol, Extracellular Region, Nucleus	structural molecule activity
Q06203	PUR1	Amidophosphoribosyltransferase	PPAT	Cytosol	Allosteric Enzyme, Glycosyltransferase Transferase
UniProtKB	Protein Symbol	Protein Name	Gene Name	Location	Function
P22102	PUR2	Trifunctional purine biosynthetic protein adenosine-3	GART	Cytosol, Extracellular Region	Ligase, Multifunctional Enzyme, Transferase
O15067	PUR4	Phosphoribosylformylglycinamide synthase	PFAS	Cytoplasm	Ligase
P22234	PUR6	Multifunctional protein ADE2	PAICS	Cytosol, Extracellular Region, Cytoplasm, Membrane	Multifunctional Enzyme, Lyase, Ligase, Decarboxylase
P30566	PUR8	Adenylosuccinate lyase	ADSL	Cytosol	Lyase
P31939	PUR9	Bifunctional purine biosynthesis protein PURH	ATIC	Cytosol, Plasma Membrane, Extracellular Region, Membrane	Hydrolase, Multifunctional Enzyme, Transferase
P15153	RAC2	Ras-related C3 botulinum toxin substrate 2	RAC2	Cytoplasm	GTP-binding, Nucleotide-binding
O75628	REM1	GTP-binding protein REM 1	REM1	Plasma Membrane	Calmodulin-binding
P61353	RL27	60S ribosomal protein L27	RPL27	Endoplasmic Reticulum, Cytoplasm	Ribonucleoprotein, Ribosomal Protein
Q9H2W6	RM46	39S ribosomal protein L46, mitochondrial	MRPL46	Mitochondrion	Ribonucleoprotein, Ribosomal Protein
P62875	RPAB5	DNA-directed RNA polymerases I, II, and III subunit RPABC5	POLR2L	Nucleus, DNA-directed RNA Polymerase	Transcription

ENO1 expression in ovarian cancer cells

Q9Y3I0	RTCB	tRNA-splicing ligase RtcB homolog	RTCB	Nucleus, Cytoplasm	Ligase
Q9NVA2	SEP11	Septin-11	SEPT11	Cytoplasm, Cytoskeleton, Synapse, Cell Junction, Cell Projection	Cell Cycle, Cell Division
Q99719	SEPT5	Septin-5	SEPT5	Cytoplasm, Cytoskeleton	Cell Cycle, Cell Division
Q9UIU6	SIX4	Homeobox protein SIX4	SIX4	Nucleus, Cytoplasm	Developmental Protein, DNA-binding
Q96GM5	SMRD1	SWI/SNF-related, matrix-associated actin-dependent regulator of chromatin subfamily D member 1	SMARCD1	Nucleus	Chromatin regulator
Q9HAU4	SMUF2	E3 ubiquitin-protein ligase SMURF2	SMURF2	Nucleus, Membrane, Cell Membrane, Cytoplasm	Transferase
P54920	SNAA	Alpha-soluble NSF attachment protein	NAPA	Cell Membrane, Membrane	ER-Golgi Transport, Protein Transport, Transport
P36952	SPB5	Serpin B5	SER-PINB5	Extracellular Region	Serine-type endopeptidase inhibitor activity
P19623	SPEE	Spermidine synthase	SRM	Cytosol	Transferase
O43295	SRGP3	SLIT-ROBO Rho GTPase-activating protein 3	SRGAP3	Cytosol	GTPase-activation
UniProtKB	Protein Symbol	Protein Name	Gene Name	Location	Function
P31948	STIP1	Stress-induced-phosphoprotein 1	STIP1	Cytoplasm, Nucleus	Mediates the association of the molecular chaperones
Q9Y3F4	STRAP	Serine/threonine kinase receptor-associated protein	STRAP	Nucleus, Cytoplasm	mRNA Processing, mRNA Splicing
P17600	SYN1	Synapsin-1	SYN1	Golgi Apparatus, Synapse, Cell Junction	Actin-binding
P54577	SYC	Tyrosine-tRNA ligase, cytoplasmic	YARS	Cytoplasm	Aminoacyl-tRNA Synthetase, Ligase, RNA-binding, tRNA-binding
Q9H4B7	TBB1	Tubulin beta-1 chain	TUBB1	Cytoplasm, Cytoskeleton, Microtubule	GTP-binding, Nucleotide-binding
Q99832	TCPH	T-complex protein 1 subunit eta	CCT7	Cytoplasm	Chaperone
P40227	TCPZ	T-complex protein 1 subunit zeta	CCT6A	Cytoplasm	Chaperone
Q59G49	TIA1	TIA1 cytotoxic granule-associated RNA-binding protein-like 1	N/A	Nucleus	RNA-binding
Q01085	TIAR	Nucleolysin TIAR	TIAL1	Nucleus, Cytoplasm	RNA-binding
P16035	TIMP2	Metalloproteinase inhibitor 2	TIMP2	Extracellular Region	Metalloenzyme Inhibitor, Metalloprotease Inhibitor, Protease Inhibitor
Q8WZ42	TITIN	Titin	TTN	Cytoplasm, Nucleus	Calmodulin-binding, Kinase, Serine/Threonine-protein Kinase, Transferase
P01375	TNFA	Tumor necrosis factor	TNF	Cell Membrane, Membrane, Extracellular Region	Cytokine
P07477/ P35030	TRY1/ TRY3	Trypsin-1/Trypsin-3	PRSS1/ PRSS3	Extracellular Region	Hydrolase, Protease, Serine Protease
Q99816	TS101	Tumor susceptibility gene 101 protein	TSG101	Cytoplasm, Cytoskeleton, Endosome, Membrane, Nucleus	Cell Cycle, Cell Division, Growth Regulation, Host-virus Interaction, Protein Transport, Transport
Q15672	TWST1	Twist-related protein 1	TWIST1	Nucleus	Activator, Developmental Protein, DNA-binding, Repressor
Q9UK80	UBP21	Ubiquitin carboxyl-terminal hydrolase 21	USP21	Nucleus, Cytoplasm	Activator, Chromatin Regulator, Hydrolase, Protease, Thiol Protease
P09936	UCHL1	Ubiquitin carboxyl-terminal hydrolase isozyme L1	UCHL1	Endoplasmic Reticulum, Membrane, Cytoplasm	Hydrolase, Ligase, Protease, Thiol Protease
O60701	UGDH	UDP-glucose 6-dehydrogenase	UGDH	Cytosol, Extracellular Region, Nucleus	Allosteric Enzyme, Oxidoreductase
P67809	YBOX1	Nuclease-sensitive element-binding protein 1	YBX1	Nucleus, Cytoplasm, Extracellular Region	Activator, DNA-binding, Mitogen, Repressor, RNA-binding

ENO1 expression in ovarian cancer cells

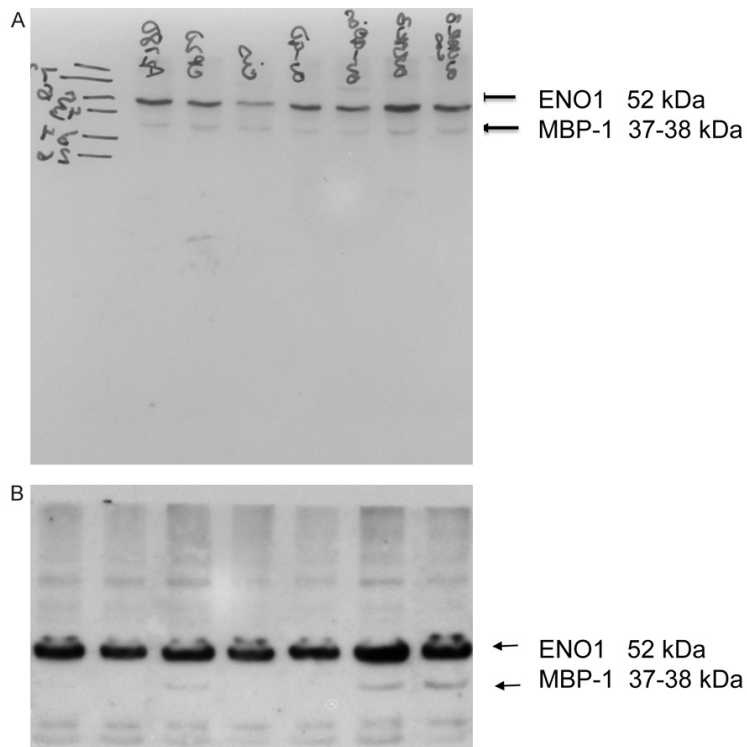
Supplementary Table 2. List of the 48 proteins differentially abundant in A280 vs. A2780CP20 cells

Gene Name	Protein Name	Ratio (A2780CP20/A280)
ACOT7	Cytosolic acyl coenzyme A thioester hydrolase	-1.390
ALDH7A1	Alpha-aminoadipic semialdehyde dehydrogenase	2.740
ALDOA	Fructose-bisphosphate aldose A	2.690
ASNS	Asparagine synthetase [glutamine-hydrolyzing]	-1.920
ATIC	Bifunctional purine biosynthesis protein PURH	-1.350
ATP5F1A	ATP synthase subunit alpha, mitochondrial	1.610
BANF1	Barrier-to-autointegration factor	2.680
CAP1	Adenylyl cyclase-associated protein 1	-1.660
CAPZA1	F-actin-capping protein subunit alpha-1	-1.64
CAZA1	F-actin-capping protein subunit alpha-1	-1.640
CCT6A	T-complex protein 1 subunit zeta	-1.120
CCT7	T-complex protein 1 subunit eta	2.260
CSTB	Cystatin-B	-2.670
DDT	D-dopachrome decarboxylase	5.070
EIF2S1	Eukaryotic translation inhibition factor 2 subunit 1	-1.460
ENAH	Protein enabled homolog	-1.430
ENO1	Alpha-enolase	-2.690
GLUD1	Glutamate dehydrogenase 1, mitochondrial	2.380
HDGF	Hepatoma-derived growth factor	-1.360
HNRNPC	Heterogeneous nuclear ribonucleoprotein C1/C2	-1.420
ILKAP	Integrin-linked kinase-associated serine/threonine phosphatase 2C	-2.520
IMPDH2	Inosine-5'-monophosphate dehydrogenase 2	-1.510
LMNA	Prelamin-A/C	-1.600
MDH1	Malate dehydrogenase, cytoplasmic	-1.260
MRPL46	39S ribosomal protein L46, mitochondrial	1.620
NAPA	Alpha-soluble NSF attachment protein	-1.540
PAICS	Multifunctional protein ADE2	-1.880
PEX19	Peroxisomal biogenesis factor 19	-1.440
PFN1	Profilin-1	-1.540
PGD	6-phosphogluconate dehydrogenase, decarboxylating	-2.010
PPP1R7	Protein phosphatase 1 regulatory subunit 7	-1.470
PRDX6	Peroxiredoxin-6	2.780
PSMD13	26S proteasome non-ATPase regulatory subunit 13	-1.430
RPL27	60S ribosomal protein L27	4.340
RTCB	tRNA-splicing ligase homolog	1.910
SEPT11	Septin-11	-2.450
SRM	Spermidine synthase	-1.420
STIP1	Stress-induced-phosphoprotein 1	-2.250
STRAP	serine/threonine kinase receptor associated protein	-1.460
TIA1	TIA1 cytotoxic granule-associated RNA-binding protein-like1	-1.970
TRY3	Trypsin-3	-1.460
TTN	Titin	2.460
TUFM	Elongation factor Tu, mitochondrial	-1.290
UCHL1	Ubiquitin carboxyl-terminal hydrolase 21	-1.570
UGDH	UDP-glucose 6-dehydrogenase	1.690
YARS	tyrosyl-tRNA synthetase	-1.780
YBX1	Nuclease-sensitive element-binding protein 1	-1.740
YWHAE	14-3-3 protein epsilon	-1.730

ENO1 expression in ovarian cancer cells

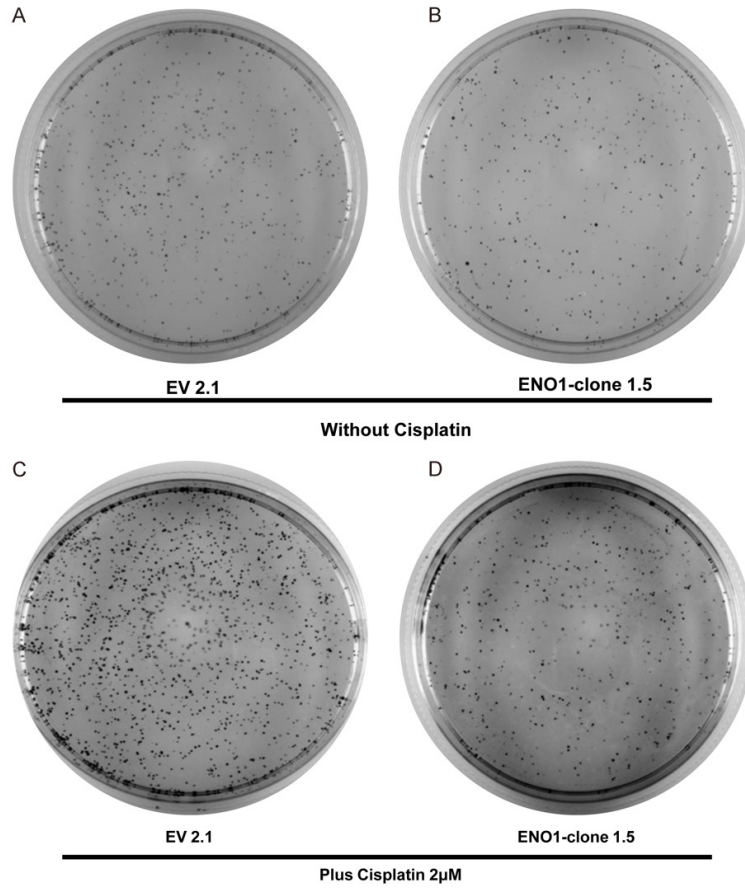
Supplementary Table 3. Concentrations of cisplatin inhibiting 50% of cell viability. Incubation with cisplatin: 72-hr following by Alamar Blue assay

Cell line	IC ₅₀ cisplatin (μM)
A2780	0.5-0.8
A2780CP20	20-30
A2780CIS	4.3
OV90	3.5
OV90CIS	9.9
OVCAR3	2.8
OVCAR3CIS	12.6



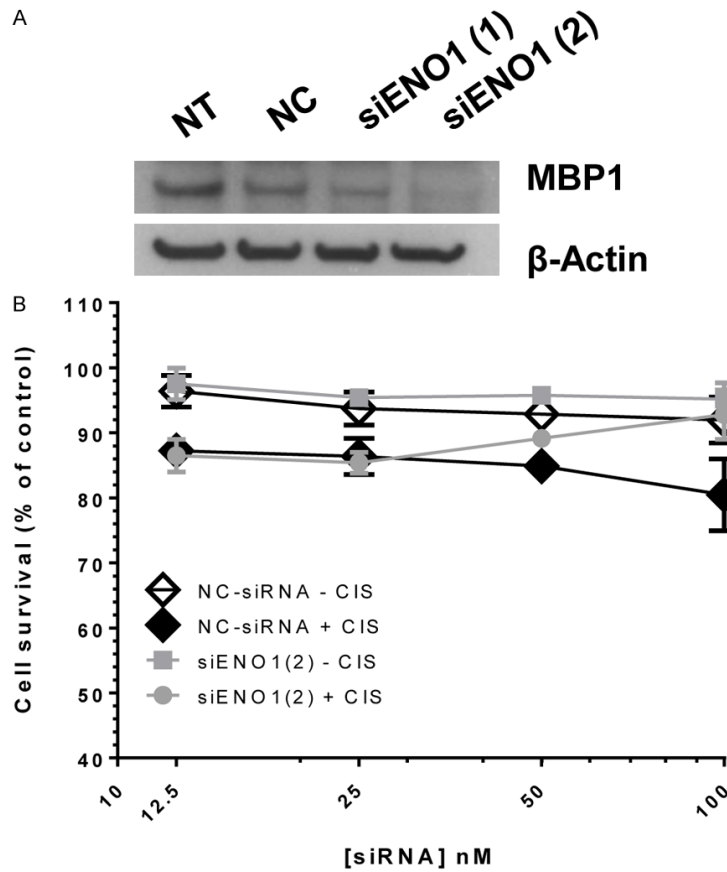
Supplementary Figure 1. Western blot images. A. Original Western blots showing the ENO1 and MBP-1 levels in the ovarian cancer cell panel. B. Western blot image showing the ENO1 and MBP-1 levels in the stable transfected clones. To observe a MBP-1 band we overexposed the X-ray film (30 minutes).

ENO1 expression in ovarian cancer cells



Supplementary Figure 2. Colony formation assays. Images of whole Petri dishes showed in **Figure 3C**. Experiments were performed as described in the legend of **Figure 3**.

ENO1 expression in ovarian cancer cells



Supplementary Figure 3. In vitro effect of siRNA-mediated ENO1/MBP-1 silencing on cell viability. A. A2780 cells (3×10^4 cells/ml) were transiently transfected with siRNAs as described in the section of “Materials and Methods” section. The band in the Western blot correspond to MBP1 (MW: 37 kDa). The ENO1-siRNA(1) had not visible effects in the MBP1 levels. However the ENO1-siRNA(2) decreased the MBP1 levels as expected. B. A2780 cells (3×10^4 cells/ml) cells were plated in 96-wells and the next day cells were transfected with siRNAs as described in the legend of **Figure 3**. Twenty-four hours after siRNA transfection different doses of cisplatin were added to the cells. Forty-eight hours later cell viability was assessed as described in the “Materials and Methods” section. Averages \pm SEM are shown for three independent experiments. The siENO1(2) which target both ENO1 and MBP-1 did not have significant effects of the sensitivity of cells to cisplatin (CIS) treatment.

